Impact of battery electric vehicle penetration and corresponding changes in upstream processes on summer O3 concentrations in Japan

Satoko Kayaba[1] and Mizuo Kajino[2]

[1]University of Tsukuba
[2]Meteorological Research Institute

November 23, 2022

Abstract

A regional meteorology–chemistry model was used to assess the effects of passenger car conversion to battery electric vehicles (BEV) on summer O3 concentrations in Kanto (Japan's most populous region). Four sensitivity experiments were conducted on different on-road and upstream (power plant and gas station) emission conditions. Daytime 8-h maximum O3 decreased by 3 ppb (5%) and 4 ppb (5%) in urban and inland suburbs, respectively. O3 levels decreased even in urban (VOC-limited regions) because exhaust and evaporative VOC emissions from vehicle and gas stations were reduced effectively (especially alkenes from gasoline evaporation; highly reactive in O3 formation). In the suburbs (NOx-limited regions), reduction of exhaust NOx by BEV shifting was significant, but in urban, even only evaporation measures induced almost the same O3 reduction effect as BEV shifting. The additional emissions from thermal power plants due to BEV night charging contributed little to the next day's daytime O3 on a monthly average basis. However, on some days, pollutants were stored in the upper part of the stable nighttime boundary layer and could affect the surface O3 as the next day's mixed layer development. Depending on the O3 sensitivity regime (NOx- or VOC-limited), additional NOx plumes from rural (urban) power plants tended to increase (decrease) the next day's O3. However, the distribution of the regime changes temporally and spatially. The H2O2/HNO3 ratio was discovered to be a clear indicator for distinguishing regime boundaries and was effective in predicting positive or negative O3 sensitivity to the additional emissions from power plants.

Impact of battery electric vehicle penetration and corresponding changes in upstream processes on summer O_3 concentrations in Japan

Satoko Kayaba[1,2] and Mizuo Kajino[2,3]

[1]Graduate School of Science and Technology, University of Tsukuba, Tsukuba, Ibaraki 305-8572, Japan

[2]Meteorological Research Institute (MRI), Japan Meteorological Agency (JMA), Tsukuba, Ibaraki 305-0052, Japan

[3]Faculty of Life and Environmental Sciences, University of Tsukuba, Tsukuba, Ibaraki 305-8572, Japan

Corresponding author: Satoko KAYABA (satoko@mri-jma.go.jp)

Key Points:

- The impact of BEV penetration on summer O_3 concentrations in the Kanto region of Japan was evaluated
- Daytime O_3 decreased in both urban and inland suburban areas
- Additional NO_x emission from power plants due to night charging for BEV affected next day daytime O_3 depending on meteorological conditions

Abstract

A regional meteorology–chemistry model was used to assess the effects of passenger car conversion to battery electric vehicles (BEV) on summer O_3 concentrations in Kanto (Japan's most populous region). Four sensitivity experiments were conducted on different on-road and upstream (power plant and gas station) emission conditions. Daytime 8-h maximum O_3 decreased by 3 ppb (5%) and 4 ppb (5%) in urban and inland suburbs, respectively. O_3 levels decreased even in urban (VOC-limited regions) because exhaust and evaporative VOC emissions from vehicle and gas stations were reduced effectively (especially alkenes from gasoline evaporation; highly reactive in O_3 formation). In the suburbs (NO_x-limited regions), reduction of exhaust NO_x by BEV shifting was significant, but in urban, even only evaporation measures induced almost the same O_3 reduction effect as BEV shifting. The additional emissions from thermal power plants due to BEV night charging contributed little to the next day's daytime O_3 on a monthly average basis. However, on some days, pollutants were stored in the upper part of the stable nighttime boundary layer and could affect the surface O_3 as the next day's mixed layer development. Depending on the O_3 sensitivity regime (NO_x- or VOC-limited), additional NO_x plumes from rural (urban) power plants tended to increase (decrease) the next day's O_3. However, the distribution of the regime changes temporally and spatially. The H_2O_2/HNO_3 ratio was discovered to be a clear indicator for distinguishing regime boundaries and was effective in predicting positive or negative O_3 sensitivity to the additional emissions from power plants.

39

40 1 Introduction

41 Ozone (O_3) in surface air has adverse effects on human health, particularly in the
42 respiratory system (e.g., *Tager et al.,* 2005; *Zhang et al.,* 2019). O_3 is not only an oxidizing agent
43 by itself, but it also generates strong secondary oxidants such as ascorbic acid ozonide (AOZ)
44 when degraded by antioxidants in the body (*Tang et al.,* 2007; *Enami et al.,* 2008). Furthermore,
45 water-soluble gaseous pollutants such as SO_2 influence only the upper respiratory tract, whereas
46 O_3 reaches deep into the lungs because of its hydrophobic nature (*Schraufnagel et al.,* 2019).

47 O_3 concentration increases with the coexistence of its precursors, NO_x ($NO + NO_2$), and
48 volatile organic compounds (VOCs). VOCs are often referred to as nonmethane VOCs
49 (NMVOCs) because the reactivity of methane to produce O_3 is much lower compared to that of
50 other VOCs in urban atmospheres. In Japan, NOx and VOC emissions and atmospheric
51 concentrations continue to plummet and the trend of O_3 concentration has been flat recently after
52 a period of reduction (*Ito et al.,* 2021). A factor is the reduction ratio of NO_x to VOCs. For
53 example, if the rate of VOC reduction is lower than that of NO_x in a VOC-limited region, such as
54 an urban area, O_3 may not reduce or could increase.

55 Vehicle transport is one of the major sources of O_3 precursors, but exhaust emission
56 levels have been reduced to approximately 1/100 of those in the 1960s, before the introduction of
57 exhaust gas regulations in Japan (*CEC,* 2022). This has been achieved by technological
58 innovations such as three-way catalysts and diesel particulate filters and by the efforts of
59 manufacturers. Alternatively, the regulations for fuel evaporation VOCs are less stringent in
60 Japan than in the United States and European countries (*Uchida,* 2016*; Tonokura and Hata,*
61 2020). Evaporative VOCs from the automotive-related sectors come from four sources: running
62 loss (RL), hot soak loss (HSL; caused by leakage from pipes within an hour after stopping),
63 diurnal breathing loss (DBL; caused by the pressure difference in the tank due to changes in
64 outside temperature during long periods of parking), and fuel evaporation during refueling.
65 These evaporative emissions are not associated with diesel but are remarkable for highly volatile
66 gasoline fuel. In Japan, there are no regulations for RL, whereas in the United States, there are
67 regulations for RL. HSL and DBL regulations have been introduced, but the time of testing
68 differs among countries. For example, in the United States, Europe, and China, the DBL emitted

during 48 h is measured, whereas in Japan, it is measured during 24 h (*Uchida,* 2016). Onboard Refueling Vapor Recovery (ORVR) on the vehicle side and Stage 1 (unloading tanks) and Stage 2 (supplying fuel) on the service station side are two measures to prevent fuel evaporation during refueling. In Japan, no regulation has been introduced for either the vehicle side or the service station side (Stage 1 is widely used in some prefectures). Although VOC emissions from stationary sources have been decreasing, emission reductions from service stations have not progressed as much as those from other sources and their relative contribution is increasing (*CEC,* 2017).

Battery electric vehicles (BEVs) are expected to become more prominent in the future. This will lead to changes in emissions not only from vehicle exhaust but also from fuel evaporation and upstream processes. BEVs have zero emissions of exhaust and fuel evaporation VOCs on-road, but they increase NO_x emissions from thermal power plants if not charged with renewable energy. Alternatively, VOC evaporation from gas stations will be reduced because of reduced fueling opportunities. The impact of vehicle electrification on O_3 concentrations has been evaluated in the United States (*Thompson,* 2009*; Nopmongcol et al.,* 2017*; Pan et al.,* 2019*; Schnell et al.,* 2019), Spain (*Soret et al.,* 2014), China (*Ke et al.,* 2016), Taiwan (*Li et al.,* 2016), and Japan (*Hata and Tonokura*, 2019). Most of them reported a similar result that the BEV penetration decreased O_3 concentrations in suburban areas (generally NO_x-limited regions) while increasing them in some urban areas and along roadsides (generally VOC-limited regions). *Nopmongcol et al.* (2017) demonstrated the results of O_3 reduction in Los Angeles, an urban area, but this assumed that off-road vehicles are also electrified, which contributed to VOC emission reduction. *Hata and Tonokura* (2019) evaluated the impact of hybrid electric vehicle or zero-emission vehicle (ZEV) penetration in Japan on summer O_3 concentrations. They reported that converting all vehicles (including trucks and buses) to ZEVs increased O_3 levels in urban centers. However, if only passenger cars were converted to ZEVs, daytime O_3 levels in urban centers decreased.

The results of these previous studies indicate that the O_3 sensitivity of BEV penetration depends on the following: "baseline emission of NO_x and VOCs in the target area (which are affected by other sources and emission controls)," "reduction ratio of NO_x and VOCs," and "O_3 sensitivity regime (NO_x- or VOC-limited) in the target area." Only a few of the previous studies have examined emission changes in upstream processes. *Hata and Tonokura* (2019) considered

emission changes from fueling stations but did not consider emission changes from power plants. In this study, we evaluated the impact of passenger car BEV shift on summer O_3 concentrations in Japan using a regional meteorology–chemistry model while accounting for upstream (power plant and gas station) emission changes.

Section 2 describes the methodology, including an overview of the CTM, observation data for model evaluation, and the sensitivity experiment assumptions. Section 3 contains the results and discussion of the model evaluation, the impact of BEV penetration on O_3 concentrations, and the impact of additional power plant emissions for BEV charging on O_3 concentrations. Section 4 finally discusses the conclusions and future works.

2 Materials and Methods

2.1 Regional meteorology–chemistry model

A regional-scale nonhydrostatic meteorology–chemistry model (NHM-Chem) (*Kajino et al., 2019; Kajino et al., 2021*) was used in this study. Detail descriptions are summarized in Table S1.

Figure 1 shows the model calculation domain in this study. The mother domain (domain 01) covered the Northeast Asian region and was calculated with dx = 30 km. The nested domain (domain 02) covered the Japanese region from Kyushu to Tohoku and was calculated with dx = 6 km. The vertical layer was 40 layers up to an altitude of approximately 20 km in both domains. Subsequently, model results refer to mixing ratios at the lowest level (approximately 15 m above ground level) unless altitude is specifically mentioned. The target period of this study was from July 1 to 31, 2015, and the simulations were integrated from June 26, with a spin-up period of five days. Summer is a season with the highest O_3 concentrations observed in Japan due to high solar radiation. Furthermore, the contribution of transboundary transport from East Asia is relatively low in summer compared to spring, so the contribution of domestic sources is high. Therefore, July was chosen as the target period because the O_3 concentration is considered the most sensitive to BEV penetration in Japan.

We used REASv3.2.1 (minor revision in December 2021 from v3.2 (*Kurokawa and Ohara, 2020*), 0.25° × 0.25°, base year = 2015) for anthropogenic emission for Northeast Asia and PM2.5EI (*Morikawa, 2017*, 1 km × 1 km, base year = 2012) for Japan. The NO_x emissions were allocated 9:1 to NO and NO_2 for both REASv3.2.1 and PM2.5EI. The VOC speciation of

REASv3.2.1 was recategorized to those of the chemical reaction mechanism (SAPRC99; *Carter,* 2000) for both REASv3.2.1 and PM2.5EI. PM2.5EI is excellent in its detailed categorization and estimation of vehicle emissions. Emissions were estimated using statistical data of traffic volume and average vehicle speed by the time of day and weekday/weekend. Furthermore, emissions were estimated for 120 categories, combining eight vehicle types (mini passenger car, passenger car, bus, light-duty truck, heavy-duty truck, special use truck, and motorcycle), five emission processes (running, start, RL, HSL and DBL), and three fuel types (gasoline, diesel, and LPG). At the smokestack altitude, power plants release pollutants. Taking chimney elevation into account, emissions from industries and power plants were distributed in this study from 0 to 300 m above the ground level. For domain 1 with Japan and domain 2 without Japan, REASv3.2.1 was used (i.e., Korea). For domain 2 over Japan, PM2.5EI was used. EAGrid (*Fukui et al.,* 2014; *Kannari et al.,* 2007) was used instead because ship emissions are not available in PM2.5EI. GFED v4 (*Giglio et al.,* 2013) was used for biomass burning emissions, and JMA observation data were used for volcanic SO_2 emissions. Biogenic VOC emissions were inline calculated based on MEGAN v2 (*Guenther et al.,* 2006) as a function of temperature and solar radiation.

For the initial and boundary conditions for the NHM (meteorological model part of NHM-Chem), we used a 6-hourly JRA-55 global reanalysis dataset (*Kobayashi et al.,* 2015) for domain 01 and 3-hourly JMA's Meso-Regional Objective Analysis (MA) for domain 02 (https://www.jma.go.jp/jma/jma-eng/jma-center/nwp/nwp-top.htm, last accessed: 30 July 2022). Spectral nudging above a height of 7 km was applied for the large-scale wave components of horizontal momentum and potential temperature (wavelength > 1,000 km), with a weighting factor of 0.06. For the chemical transport model (CTM) part of NHM-Chem, monthly climatological values were used for the initial and boundary concentrations of domain 01 and the results of domain 01 were used for domain 02. The input/output time interval of CTM was 1 h.

2.2 Model experimental cases and parameter settings

2.2.1 Emission scenarios

As shown in Table 1, four model experiments (or emission scenarios) were conducted in this study. Heavy-duty vehicles and motorcycles were assumed to be nonelectric. The assumptions of total vehicle ownership and activity were not changed in the sensitivity experiment to evaluate the sensitivity to changes in emission factors.

(1) “BASE” experiment

This is a replicated experiment of the current situation based on the meteorological field in 2015. Emissions are based on each inventory (Table S1).

(2) “All BEV” experiment

All passenger cars are shifted to BEVs. All BEV charging is conducted at night (23:00–8:00) to level out demand. During this period, additional emissions from thermal power plants are produced.

(3) “All BEV (PP unchanged)” experiment

All passenger cars are shifted to BEVs, with power plant (PP) emissions unchanged (assumed 100% supplied by renewable energies). The difference between (2) and (3) indicates the sensitivity of additional power plant emissions.

(4) “Evapo reduce” experiment

Only evaporative NMVOCs emitted by passenger vehicles and gas stations are reduced (passenger car exhaust remains unchanged). This is the situation when only evaporation measures are conducted without BEV penetration.

2.2.2 Changes in upstream emissions due to BEV penetration

Figure S1 demonstrates the diurnal additional electricity demand for BEV charging. We assumed normal nighttime charging for all BEVs because a large percentage of BEV users currently charge late-night electricity at home (*MLIT urban bureau,* 2012). The load due to increased demand is assumed to be charge-controlled to level out. Thermal power plant emissions increase during the 9 h period (from 23:00 to 8:00). The increased electricity demand for BEV charging is derived to be 71.4 billion kWh/year, assuming an average electricity consumption of 0.17 kWh/km for BEVs and a total annual passenger car travel volume of 420 billion km/year (*MLIT,* 2010). This increased demand corresponds to approximately 7% of total electricity demand (1077.8 billion kWh/year), which will be met by nighttime baseload and middle power (90% thermal and 10% hydro in 2012, the base year for the PM2.5EI). The emissions from the thermal power plant for this 9 h period would increase by approximately 25%–30%, assuming that plant emissions are proportional to the amount of electricity generated. In reality, emissions will not increase proportionately with the increased generation because

generation efficiency will increase. However, in the same manner, as in previous studies (*Thompson et al.*, 2011; *Soret et al.,* 2014; *Ke et al.,* 2016; *Li et al.,* 2016; *Schnell et al.,* 2019), we assumed proportional to this study because no information regarding the relationship among power generation, generation efficiency, and emissions was available. The power grid in Japan is assumed to be uniform. In reality, LNG-fired power would be applied as the marginal power, but coal, oil, and LNG-fired power were assumed to increase uniformly.

The evaporation NMVOCs is assumed to be reduced by 80% because BEV penetration will reduce refueling frequency. Here 80% is the share of gasoline consumption by passenger cars to that of total (*MLIT,* 2012). Although emission changes at refineries should be considered as well as power plants and gas stations, it was assumed to be unchanged in this study. Because estimating the change in crude oil refining volume is difficult (not only gasoline demand but also other petroleum products will be involved).

2.3 Observation data for model validation

The Ministry of the Environment, Japan (MOEJ)'s wide area monitoring data for air pollutants (Atmospheric Environmental Regional Observation System: AEROS) were used to validate the simulation results of O_3 concentrations. The concentrations of SO_2, NO, NO_2, Ox, CO, NMHC, CH_4, THHC, SPM, and $PM_{2.5}$ are monitored hourly every day at approximately 1900 measuring stations throughout Japan (some substances are not measured at some stations). The National Institute for Environmental Studies screens out anomalous data from those preliminary values and publishes confirmed data. Confirmed data were used in this study. We generated super observation data by simply averaging the hourly observation data of observation sites in each model grid (dx = 6 km) to compare against the simulation results. In the Kanto region, there are 234 super observation grids.

3 Results and Discussion

3.1 Model evaluation

Comparative statistics between the model BASE experiment and observations with daily average O_3 and MDA8h O_3 (daily maximum 8 h average O_3) are shown in Table 2. The top two rows are the Kanto area (Figure 1) averaged data for 31 days. The correlation coefficients of these data indicate day-by-day temporal correlations because the diurnal variation of O_3 is smoothed out. The correlation coefficients are higher for both daily average O_3 and MDA8h O_3 ($R = 0.66$ and 0.79, respectively), indicating that the model accurately reproduced the temporal variability of daily high concentration events affected by weather conditions. The bottom two rows are July monthly averaged data for the nationwide 864 super observation grids (all of domain 2, Figure 1). The correlation coefficients of these data indicate the spatial correlations. They show a moderate correlation ($R = 0.32$ and 0.56 for daily average O_3 and MDA8h O_3, respectively). This is because the highest O_3 concentration was distributed in Kanto inland in the model's result, whereas in the observation data, it was distributed in Kyushu and Chugoku. However, within only Kanto ($N = 234$), the correlation coefficient was higher ($R = 0.6$). The model reproduced the distribution of the O_3 concentration gradient from the coastal to the inland areas of the Kanto region relatively well.

The simulated MDA8h O_3 over Kanto was slightly overestimated (NMB = 3.6%) probably because of the overestimation of photochemical production. Alternatively, the simulated daily average O_3 concentration is slightly underestimated (NMB = −9.7%) probably because of a slight overestimation of the nighttime NO titration (Figure S2).

3.2 Impact of passenger cars shifting to BEVs on daytime O_3 concentration

3.2.1 Results of passenger car "all BEV" experiments

Figure 2 shows NO_x and NMVOC emissions in the BASE experiment (Figure 2a, d) and their change with the shift of all passenger cars to BEVs (i.e., (2) All BEV experiment — (1) BASE experiment). Figure 3 shows the diurnal variation of these emissions in major sources

(Figure 2 area (A)). The industry sector is the largest NO_x emission source, followed by heavy-duty vehicles during the daytime. The contribution of passenger car emissions was low (Figure 3a). NO_x emission was reduced by up to 10%–15% by BEV shifting during urban commuting hours (Figure 2b), that is, approximately −5% during daytime area (A) average (Figure 3b). It increases approximately 5% net for the nighttime area (A) average (Figure 3b). At night, emissions increase from thermal power plants, and they decrease from passenger cars, but the effect is small because of low traffic volumes (Figure 2c).

Although higher biogenic NMVOC emissions in July, anthropogenic NMVOC emissions accounted for approximately 90% of total NMVOC emissions in urban areas (Figure 2e). It is mainly from stationary sources such as the painting industry (Figure 3c). The NMVOC emission was reduced by approximately 10% by BEV shifting for the area (A) average (Figure 3d), owing to a reduction in three sources: passenger car exhaust, passenger car evaporation, and gas station evaporation.

Figure 4a shows the July average of MDA8h O_3 concentrations in the BASE experiment. High O_3 concentration is distributed inland along the topography is because precursors emitted in the urban coastal areas are transported by sea breezes (e.g., *Ooka et al.,* 2011). The MDA8h O_3 sensitivity by BEV shifting was also large inland, with a maximum of approximately −5 ppb (−5%) (Figure 4b).

Figure 4c shows the MDA8h O_3 sensitivity when only fuel evaporation measures for passenger cars and gas stations are taken (i.e., (4) Evapo reduce experiment — (1) BASE experiment). The reduction rate is almost the same as that in Figure 4b even without reducing vehicle exhaust in Tokyo and the southern part of Saitama because these areas are VOC-limited regions. Because there is a time lag before BEVs are widely spread in the real world, it is effective to implement ahead with fuel evaporation measures to reduce urban O_3. Specifically, Stage 2 (add a gas recovery system to the refueling pump and return it to an underground tank) and ORVR (add a gas adsorption system with activated carbon sealed to the vehicle) are the main measures during refueling. Changing the rubber material of the vehicle pipe to one that is less permeable and increasing the capacity of the gas adsorption system are the main parking measures. Among these, Stage 2 is estimated to be cost-effective (*CEC,* 2017). Furthermore, the effect of Stage 2 in reducing summer O_3 concentration in Kanto was demonstrated using an atmospheric model (*Nakagawa et al.,* 2019). Therefore, it is considered an effective measure.

Conversely, it was also suggested that reducing NO_x emissions in urban areas is important to reduce high concentrations of O_3 inland (NO_x-limited region) and that BEV penetration can benefit from this (Figure 4b, c).

3.2.2 O_3 formation potential of NMVOCs

The reactivity of NMVOCs for O_3 formation varies according to species. In this section, we quantify the relative contributions of species and sources to the reduction of O_3, as presented in Section 3.2.1.

Figure 5a depicts the emissions of NMVOCs in Area (A) (Figure 2) as well as the amount of reduction due to BEV shift. Figure 5b depicts the breakdown of the contribution of each species and source to the reduction. The NMVOC composition of exhaust and gasoline fuel evaporation is shown in Figure S3. The composition of gasoline and diesel exhaust gas components is based on data from a tunnel survey conducted in Tokyo in 2010 (*Uchida et al.,* 2013). The gasoline vehicle exhaust was dominated by alkanes (approximately 50%), followed by aromatics (approximately 40%) and alkenes (approximately 9%) (Figure S3a). The NMVOC composition of gasoline fuel evaporation is based on data from the DBL test (*Yamada et al.,* 2015a). The species from permeation (leak gas from the rubber pipe of the vehicle) are alkanes (55%), aromatics (25%), and alkenes (20%) (Figure S3c). Alternatively, the species from breakthrough (leak evaporative gas in the fuel tank when over the capacity of the canister) are alkanes (68%) and alkenes (32%) and do not include aromatics (*Yamada et al.,* 2015a) (Figure S3d). This is because species with low molecular weight and high volatility dominate in evaporative gas in the tank (*Hagino et al.,* 2015). Permeation species predominate in RL, HSL, and the first day of DBL, whereas breakthrough species predominate after the second day of DBL (*Yamada et al.,* 2015a; *Hagino et al.,* 2015). Therefore, in this study, permeation data from the DBL test are adopted for RL and HSL and breakthrough data are adopted for DBL.

The composition of refueling evaporation is also composed of alkanes (75%) and alkenes (23%), as shown in Figure S3e (*Yamada et al.,* 2015b). It lacks aromatics for the same reason that a breakthrough does. Additionally, the test by *Yamada et al.* (2015a and 2015b) was conducted under 20°C conditions. However, it has been reported that the NMVOC composition

of refueling evaporative gas remained unchanged when the temperature was increased from 10°C, 25°C, to 30°C (*Hagino et al.,* 2015).

The emissions of NMVOC mass were reduced by approximately 10% in Area (A) by BEV shifting (Figure 5a). The most reduced of these was alkane (65% contribution). By the source, passenger car exhaust gas, passenger car fuel evaporation, and gas station fuel evaporation contributed roughly 4:3:3 to the mass reduction of NMVOCs (Figure 5b).

Figures 5c and 5d are the same as Figures 5a and 5b but for ozone formation potential (OFP), which considers the reactivity of each NMVOC species. OFP is derived by Equation (1), which is calculated by weighting NMVOC emissions by MIR, the reactivity index of O_3 production.

$$OFP_i = E_i \times MIR_i, \qquad (1)$$

where OFP_i is the O_3 formation potential of NMVOC species i (g-O_3 h^{-1}), E_i is the emission of NMVOC species i (g-NMVOC h^{-1}), and MIR_i is the maximum incremental reactivity of NMVOC species i (g-O_3/g−NMVOC). The MIR values are displayed in Table S2, which are based on *Carter* (2000). *Carter* (2000) derived these MIR values by conducting sensitivity experiments using the box model of the SAPRC-99 chemical module.

The OH reaction rate constant (kOH) (*Atkinson,* 1994; *Atkinson,* 1997; *Atkinson,* 2000) is an index for comparing the reactivity of NMVOC species. Although MIR was employed in this study because MIR is superior in that it can consider the effects of secondary reactions, which kOH cannot. More specifically, kOH represents only the initial OH reactivity in the RO_x cycle and cannot account for differences in reactivity between RO_2 and NO produced after that. As a result, there is a concern that it overestimates the impact of NMVOC species that react quickly with OH but do not produce a significant amount of O_3 in subsequent reactions (or vice versa) (*Carter,* 1994; *Tajima et al.,* 2010).

The OFP decreased approximately 5.5% in Area (A) by BEV shifting, slightly less than the mass-based reduction (Figure 5c). This is due to the lower MIR of alkanes, which contributed the most to the mass-based reduction. Instead, the reduction of alkene contributed the most to OFP reduction (47% contribution) (Figure 5d). The contribution of the three sources was 4:3:3, which is consequently the same as mass-based results (Figure 5d). Overall, it was estimated that

the alkenes from passenger car and gas station fuel evaporation, as well as the aromatics from passenger car exhaust gases, contributed significantly to the O_3 reduction achieved through BEV shifting (Figure 5d). They contributed 19%, 18%, and 13% to OFP reduction, respectively.

3.3 Impact of additional emissions from a thermal power plant due to nighttime BEV charging on the next day's daytime O_3

Thermal power plants are typically located in coastal areas. A previous study based on BEV penetration in Spain ascertained that even if BEV charging increased pollutant emissions from gas-fired power generation at night, nighttime onshore winds would wash the pollutant plume seaward with no problem (*Soret et al.,* 2014). As such, the impact of additional power plant emissions may not affect residential areas. However, there could be a case that the impact is significant depending on the meteorological field and emission conditions, so we discuss it in this section. That is, evaluating the impact of additional NO_x, given that the power plant emits almost no NMVOCs (Figure 3c, d).

Figure 6a depicts the sensitivity of July mean MDA8h O_3 concentration due to additional power plant emissions (i.e., (2) All BEV experiment — (3) All BEV (PP unchanged) experiment). The areal maximum sensitivity was very low at approximately −0.5% (−0.2 ppbv) monthly. This is because the advection path of the plume and the daytime photochemical reaction rate vary depending on the daily wind pattern and solar radiation (as confirmed by the hourly O_3 sensitivity map).

However, there were some cases of relatively high sensitivity. Figure 6b depicts the case at 13:00 on July 26. Around Tokyo Bay and Lake Kasumigaura, the O_3 sensitivities are approximately −5% (−4 ppb) and +5% (+5 ppb) (area enclosed with a solid line). They were carried by additional plumes from thermal power plants in Tokyo Bay and Kashima city, respectively. Similar cases of relatively high O_3 sensitivity were discovered over several days in late July. This may be due to the high solar radiation and temperatures in late July 2015 caused by the predominance of the Pacific High, which accelerated the photochemical O_3 formation.

The positive or negative sensitivity of O_3 to such additional NO_x depends on whether the region is NO_x- or VOC-limited. Generally, the O_3 sensitivity regime is VOC-limited in urban areas and NO_x-limited in a suburb (e.g., *Sillman,* 1999). This is also the case in the Kanto region

of Japan, where the rate changes from VOC-limited to NO_x-limited as one moves from the urban center around Tokyo Bay to the inland suburbs (*Inoue et al.*, 2010a). As a result, the positive and negative O_3 sensitivities enclosed with solid lines are consistent with this trend. However, there are cases where O_3 has negative sensitivity (i.e., VOC-limited) despite living in a suburban area (area enclosed with a dashed line).

In this section, we first analyze the distribution of NO_x or VOC sensitivity regimes in such high O_3 sensitivity cases (Sec. 3.3.1). Then, the mechanism by which additional NO_x is emitted from the power plant stack to result in next day sensitivity was analyzed, focusing on the effect of atmospheric stability (Sec. 3.3.2).

3.3.1 O_3 sensitivity regime and H_2O_2/HNO_3 indicators

3.3.1.1 Radical cycle and termination process

This section provides a brief description of the O_3 formation mechanism and sensitivity regime, which will be required for the subsequent discussion. The increase in tropospheric O_3 is caused by the RO_x cycle, which is initiated by the oxidation of VOCs by OH. The RO_x cycle causes an imbalance of the NO_x cycle equilibrium ($NO_2 + O_2 \Leftrightarrow NO + O_3$) and contributes to NO_2 formation ($RO_2 + NO \rightarrow RO + NO_2$, $HO_2 + NO \rightarrow OH + NO_2$). Under high NO_x conditions, the terminal reactions are as follows, producing HNO_3 and PAN.

$NO_2 + OH \rightarrow HNO_3$ (R1)

$NO_2 + RO_2 \rightarrow RO_2NO_2$ (R2)

The additional NO_x in this situation reduces O_3 because it deprives OH available for VOC oxidation and inhibits the RO_x cycle. As a result, the O_3 concentration rises with increasing VOCs and falls with increasing NO_x, indicating that the region is a VOC-limited region.

Alternatively, under low NO_x conditions, these self-reactions among HO_2 and between HO_2 and RO_2 are the termination reactions, producing H_2O_2 and ROOH.

394 $HO_2 + HO_2 \rightarrow H_2O_2 + O_2$ (R3)

395 $HO_2 + RO_2 \rightarrow ROOH + O_2$ (R4)

396

397 Therefore, the O_3 concentration is not affected by VOCs but by the NO_x concentration,
398 indicating that the region is NO_x-limited.

399

400 On the basis of the above mechanism, the O_3 sensitivity in Figure 6b can be explained by the
401 NO_x, NO_y (all oxidized nitrogen compounds), NO_z (NO_y minus NO_x), nonmethane hydrocarbons
402 (NMHC), and NO_2/NO_x sensitivity as shown in Figure 7. Around Tokyo Bay, the positive NO_x
403 sensitivity brought by the power plant during the night remained until the next daytime (Figure
404 7a). NMHC sensitivity was positive because the additional NO_x inhibited the RO_x cycle (=
405 suppressed VOC consumption) (Figure 7d). The NO_2 formation was suppressed, NO_2/NO_x ratio
406 decreased (Figure 7e), and O_3 also decreased (Figure 6b). Alternatively, no NO_x sensitivity was
407 found around Lake Kasumigaura (Figure 7a). This is because all NO_x was converted to NO_z
408 (Figure 7c). NMHC sensitivity was negative (Figure 7d) because the additional NO_x further
409 accelerates the RO_x cycle (= accelerated VOC consumption). NO_2 production was promoted,
410 NO_2/NO_x ratio increased (Figure 7e), and O_3 also increased (Figure 6b).

411

412 3.3.1.2 H_2O_2/HNO_3 indicator for identifying the O_3 sensitivity regime

413 The grayscale in Figure 8 shows the H_2O_2/HNO_3 ratio. *Sillman* (1995) first proposed the
414 H_2O_2/HNO_3 indicator that can identify the O_3 sensitivity regime. This value is lower in the VOC-
415 limited region and higher in the NO_x-limited region. This is because, as mentioned above, the
416 main terminate products of the RO_x cycle are H_2O_2 or HNO_3 in NO_x-limited or VOC-limited
417 regions, respectively (*Sillman,* 1995; *Sillman,* 1999; *Sillman and He,* 2002).

418 The distribution of monthly mean H_2O_2/HNO_3 showed a trend of regime change from
419 urban to suburban areas (Figure 8a). However, it has been reported that the distribution of regime
420 boundary changes temporally and spatially (e.g., *Sillman,* 1999; *Martill et al.,* 2002; *Song et al.,*
421 2010; *Lei et al.,* 2007; *Kannari and Ohara,* 2010). This is because the regime is determined by
422 multiple factors, not only the NO_x/VOCs emission ratio but also photochemical aging (*Sillman,*
423 1999). Any polluted plumes immediately after being emitted are NO_x-rich and VOC-limited, but

424 over time, NO_x is removed by the process (R1, R2) and changes to NO_x-limited (*Milford et al.,*
425 1989). However, if atmospheric mixing is weak and photochemical aging is slow, the transition
426 from VOC-limited to NO_x-limited is delayed so that the VOC-limited region is expanded in the
427 downwind suburbs (e.g., *Kleinman,* 1994; *Martilli et al.*, 2002; *Spirig et al*, 2002).
428
429 This is the reason why negative O_3 sensitivity (VOC-limited) occurs in the suburban area
430 circled by the dashed line in Figure 6b.
431 In the July 26 13:00 case, the distribution of low H_2O_2/HNO_3 corresponded to negative
432 O_3 sensitivity (=VOC-limited), and high H_2O_2/HNO_3 distribution corresponded to positive O_3
433 sensitivity (=NO_x-limited) (Figure 8b). Furthermore, regime discrimination by the H_2O_2/HNO_3
434 index was successful not only in this one-hour value case but also when the region and period
435 were expanded to include the nationwide and through July. Details for an evaluation of the
436 versatility of the H_2O_2/HNO_3 index and its best threshold are presented in Appendix A. In
437 summary, depending on factors such as the rate of photochemical aging, the regime distribution
438 may not conform to the general trend of VOC-limited in urban and NO_x-limited in suburbs (even
439 suburbs can be VOC-limited). H_2O_2/HNO_3 worked as a clear indicator that could discriminate
440 such hourly changing regime boundaries and the best threshold was found as 0.5. H_2O_2/HNO_3
441 index is useful for predicting positive (where $H_2O_2/HNO_3 > 0.5$) or negative (where H_2O_2/HNO_3
442 < 0.5) O_3 sensitivity to emission changes in power plants.
443
444

445 3.3.2 Nighttime meteorology and atmospheric chemistry (atmospheric stability, effect
446 of NO titration)

447
448 Figures 9 and 10 are longitude–altitude cross-sections at 35.9°N and 35.5°N on July 26,
449 2015, respectively (cut over the point of greater sensitivity in Figure 6b). Three-hourly snapshots
450 are shown from 2:00 to 14:00 for (a) NO_x sensitivity, (b) O_3 sensitivity and H_2O_2/HNO_3 ratio,
451 and (c) PO_3 sensitivity, respectively, induced by additional power plant emissions. The
452 sensitivity of PO_3 (potential O_3) (ΔPO_3) is defined by the following equation, which indicates the
453 sensitivity of O_3 concentration due to factors other than NO titration (i.e., chemical reaction

454 generation and advection). This indicator is based on the fact that O_3 + NO_2 remains unchanged
455 even when O_3 is decomposed in NO titration.
456
457 $$\Delta[PO_3] = \Delta([O_3] + [NO_2] - 0.1 \times [NO_x]),$$
458
459 where $[PO_3]$, $[O_3]$, $[NO_2]$, and $[NO_x]$ are their respective concentrations (ppb). 0.1, the
460 coefficient on NO_x, is the NO_2 ratio in primary NO_x emissions, and the effect of primary NO_2
461 emissions is removed in this term.
462 First, we focus on the area around Lake Kasumigaura, shown in cross-section (A). From
463 2:00 to 10:00 local time, additional NO_x from the thermal power plant in Kashima city titrated
464 O_3, resulting in negative sensitivity (Figures 9a and 9b). During the night, the pollutants are
465 situated aloft in the upper part of the stable nighttime boundary layer. As the sun rose, the mixed
466 layer developed in the lower atmosphere, which resulted in positive O_3 sensitivity in the NO_x-
467 limited region (Figure 9b). At 14:00, NO_x has been completely converted to HNO_3, the
468 terminated product of the RO_x cycle, so there is no sensitivity (Figure 9a). Approximately
469 140.8°E is the shoreline. The positive O_3 sensitivity was lifted by the upwelling generated by the
470 land surface with higher surface temperatures and diffused significantly vertically within the
471 mixed layer (Figure 9b).
472 Next, we focus on the Tokyo Bay area shown in cross-section (B). As mentioned above,
473 additional NO_x from the power plants around Tokyo Bay titrated O_3 during the night (Figures
474 10a and 10b). The plume was transported westward over the top of the stable nighttime boundary
475 layer, maintaining an emission altitude of 200–300 m, and thus, remained stagnant along the
476 terrain. As the sun rose, it diffused within the mixed layer with negative O_3 sensitivity. The
477 negative O_3 sensitivity at 14:00 can be mostly explained by VOC-limited chemistry (Figures 10b
478 and 10c) because $\Delta PO_3 \approx \Delta O_3$, although there is still some contribution from the nighttime
479 titration. The distributions of negative O_3 sensitivity and low H_2O_2/HNO_3 values corresponded to
480 each (Figure 10b). This indicates that the H_2O_2/HNO_3 indicator worked not only horizontally but
481 also vertically.
482 Conversely, focusing on the negative O_3 sensitivity from the NO titration at night, the
483 H_2O_2/HNO_3 values are not lower (Figures 9b and 10b). This is because the NO titration process
484 contributes little to the terminated products of the RO_x cycle (HNO_3 and H_2O_2). This means that

485 negative O_3 sensitivity could occur if the NO titration process is dominant, even in areas
486 identified as NO_x-limited regions by the H_2O_2/HNO_3 ratio.
487 This is consistent with what is described in *Sillman and He* (2002). To distinguish the effect of
488 NO titration, it is necessary to use a different index than H_2O_2/HNO_3, such as O_3/NO_y (*Sillman*
489 *and He*, 2002).
490

491

492 4 Conclusions

493 The impact of all passenger cars shifting to BEV in Japan on O_3 concentrations in Kanto
494 during summer was evaluated by sensitivity experiments using the regional meteorology–
495 chemistry model NHM-Chem. The four sensitivity experiments were conducted under different
496 conditions for on-road and upstream (thermal power plants and gas stations) emission changes.
497 The sensitivity of passenger cars in all BEV experiments indicated that daytime O_3
498 concentrations decreased over a wide area of the Kanto, resulting in a sensitivity of up to −5%
499 (−4 ppbv) in the inland suburb following typical sea breeze transport patterns. Several previous
500 studies that evaluated the impact of BEV penetration on air quality in other countries found that
501 reduced NO_x from vehicle exhaust reduces O_3 in suburbs but increases O_3 locally in urban,
502 VOC-limited regions. In this study, however, daytime O_3 levels were reduced even in urban
503 areas. That is because BEV shifting effectively reduced NMVOCs from the three evaporation
504 sources: vehicle exhaust, vehicle evaporation, and gas station evaporation, and it is likely related
505 to the Japanese context, where most passenger cars are gasoline-powered and fuel evaporative
506 VOC emission regulations are relatively lax. These three sources contributed approximately
507 4:3:3 to the reduction of NMVOC emissions on a mass basis, with alkanes from all sources
508 contributing the most to the reduction. However, alkanes have a relatively low reactivity for O_3
509 formation. Therefore, on the basis of the ozone formation potential (OFP), which considers the
510 reactivity of NMVOC species, it was estimated that the reduction of alkenes from fuel
511 evaporation from passenger cars and gas stations, as well as aromatics from passenger car
512 exhaust, contributed significantly to the reduction of O_3. The contribution of the three NMVOC
513 sources to OFP reduction was similar to that of the mass basis, with gasoline fuel evaporation
514 contributing 60%, indicating its importance. Furthermore, it was found that only evaporation
515 measures (without reducing passenger car exhaust) induced almost the same O_3 reduction effect
516 in urban areas. Because a time lag in the real world before BEVs is widely adopted, it is
517 presumed that introducing fuel evaporation measures (such as Stage 2) ahead of time will be
518 effective for the early improvement of urban air quality. It was also suggested that NO_x reduction
519 is still important for reducing high O_3 concentrations over inland suburbs (NO_x-limited region):
520 BEV shifting is beneficial over the area.

The additional NO_x emission from the thermal power plant due to BEV's nighttime charging contributed little to the monthly average of next daytime O_3 (−0.5% at most). This is because the plume emitted from point sources has different advection paths and chemical reaction rates depending on the daily meteorological field, and O_3 sensitivity becomes random. However, on some days, O_3 sensitivity can be higher, topically ± 5%. In these cases, additional pollutants from the thermal power plant during the night were stored in the upper part of the stable nighttime boundary layer and advected while maintaining an emission altitude of 200–300 m, affecting the surface O_3 concentration at the arrival area as the mixed layer developed.

The concentration of O_3 tended to decrease (increase) in the plumes downwind of the power plant in urban (suburb) locations, which is consistent with the general distribution of O_3 sensitivity regime (VOC or NO_x) change trend from urban to suburb. However, locations of regime boundaries change temporally and spatially, depending on factors such as the photochemical aging rate of the pollution plume. There were some cases of negative O_3 sensitivity (i.e., VOC-limited) in the suburbs in this study. We discovered that an H_2O_2/HNO_3 index with a threshold of 0.5 worked as a clear indicator to distinguish the spatial distributions of regime boundaries and was effective in predicting positive or negative O_3 sensitivity to additional NO_x emissions from power plants. However, even in these regions determined to be NO_x-limited by the H_2O_2/HNO_3 index, the O_3 sensitivity was negative if the NO titration process was dominant. To distinguish negative O_3 sensitivity due to the effect of NO titration, it is necessary to use a different index than H_2O_2/HNO_3, such as O_3/NO_y.

The results in this study are similar to some of *Hata and Tonokura* (2019), a previous study that evaluated the air quality impacts of ZEV deployment in Japan for the first time. This study additionally considers changes in the power plant emissions, which they did not consider, but the impacts are not very significant every month. It was discovered, however, that it could affect diurnal O_3 concentrations topically in space and time.

In this study, sensitivity experiments were conducted to evaluate the impact of a passenger car's BEV shifting. To predict a realistic future society, scenarios must be constructed based on more realistic assumptions, such as powertrain mix, including heavy-duty vehicles, charging patterns, power source mix, and power generation efficiency, and then evaluated in a model simulation. At that time, information on future powertrain mix for heavy-duty vehicles and future emission regulation for power plants is scarce, which will lead to uncertainties.

552 Furthermore, although we focused solely on O_3 in this study, it would be desirable to conduct an
553 integrated assessment of other gaseous and particulate pollutants that have similar health effects,
554 i.e., oxidative stress on the respiratory system.

555

556

557 **Appendix A: Evaluation of H_2O_2/HNO_3 ratio as an indicator of O_3 sensitivity regime**

558 We discuss the versatility and best thresholds for the H_2O_2/HNO_3 indicator here.
559 The threshold values of the indicator have been reported in several previous studies.
560 *Sillman and He* (2002) reported that $H_2O_2/HNO_3 \leq 0.2 \sim 0.4$ at the 95th percentile value is the
561 threshold for VOC-limited and $H_2O_2/HNO_3 \geq 0.7 \sim 3.1$ for NO_x-limited, based on model
562 sensitivity experiments the United States. *Inoue et al.* (2010b) conducted a similar analysis to
563 *Sillman and He* (2002) for five summer days in Japan and reported that the VOC-limited
564 threshold is $H_2O_2/HNO_3 \leq 0.3$. Multiple sensitivity experiments using chemical transport models
565 are used to derive the threshold in these studies; NO_x and VOC emissions are varied and O_3
566 sensitivity and corresponding H_2O_2/HNO_3 are statistically analyzed for all periods/grids. This
567 study, however, did not conduct such multiple sensitivity experiments with finely tuned NO_x and
568 VOC parameters. As a result, the following methods were used to examine the versatility of the
569 H_2O_2/HNO_3 indicator and to derive the best threshold value.
570 Figure A1a shows the correct judgment rate for the O_3 sensitivity regime when the
571 H_2O_2/HNO_3 threshold is varied. The target is the grid data with $O_3 \geqq 70$ ppb and $|\Delta O_3$
572 (difference of O_3, all BEV minus all BEV (PP unchanged)) (difference of O_3, (2) All BEV
573 experiment — (3) All BEV (PP unchanged) experiment) $| \geqq 0.5$ ppb, from 10:00 to 15:00 on
574 July 1 to 31 in the national area shown in Figure A1b. In other words, develop a threshold that
575 can accurately judge positive or negative O_3 sensitivity induced by additional NO_x emissions
576 from nationwide thermal power plants.
577 The light blue graph in Figure A1a shows the percentage of negative O_3 sensitivity in the
578 data with H_2O_2/HNO_3 below the threshold (i.e., the percentage of the correct judgment of the
579 VOC-limited). The lower (tougher) the threshold value is, the higher is the correct judgment rate.
580 Furthermore, the higher the threshold value, the lower the correct judgment rate, converging to a
581 probability of 1/2 (i.e., threshold meaningless state). The light-yellow graph in Figure A1a

582 depicts the percentage of positive O_3 sensitivity in the data with H_2O_2/HNO_3 above the threshold
583 (i.e., the percentage of the correct judgment of the NO_x-limited). For thresholds that are too small,
584 this correct judgment rate will drop. For example, assume that we reduce $H_2O_2/HNO_3 = 0.1$ in
585 Figure 8b. You can image that the VOC-limited (negative O_3 sensitivity) can be filtered
586 completely but the percentage of negative O_3 sensitivity would also be higher in the data above
587 the threshold value (more miss judgment). Considering both (light blue and yellow), the best
588 threshold value was derived as $H_2O_2/HNO_3 = 0.5$ for the target data in this study. Here, both
589 NO_x- and VOC-limited could be judged with a correct response rate of approximately 90%. It
590 was determined to be adaptable even when the target area and period were expanded (Figure
591 A1a).

592 We have discussed H_2O_2/HNO_3 indicator, but various other indicators have been
593 proposed (e.g., O_3/NO_y, O_3/NO_z, O_3/HNO_3, $(H_2O_2 + ROOH)/HNO_3$, H_2O_2/NO_z, $(H_2O_2 +$
594 $ROOH)/NO_z$, H_2O_2/NO_y, and $(H_2O_2 + ROOH)/NO_y$) (*Sillman and He,* 2002). It has been noted
595 that in areas with high biogenic VOCs, the numerator should include organic peroxy radicals
596 (ROOH) in addition to H_2O_2 because the contribution of (R4) is larger in (R3, R4) (*Vermeuel et*
597 *al.,* 2019). It has also been pointed out that the denominator should be NO_z or NO_y because of
598 the NO_3 ions in the HNO_3 transition between the gas and aerosol phases (*Martilli et al.,* 2002).
599 Considering these notes, we analyzed the same for $(H_2O_2 + ROOH)/NO_z$. As a result, the trend
600 of $(H_2O_2 + ROOH)/NO_z$ distribution was generally like that of H_2O_2/HNO_3, which was also
601 confirmed to work as a judgment index for the O_3 sensitivity regime (Figure S4). The best
602 threshold value was estimated to be $(H_2O_2 + ROOH)/NO_z = 0.35$ (Figure S5).
603

Acknowledgments

The authors are thankful for Drs. Tazuko Morikawa and Hiroyuki Hagino of Japan Automobile Research Institute for providing PM2.5EI and useful comments on emission inventories and Ms. Natsumi Tanji of JMA for data processing. The authors are also thankful for Drs. Masayoshi Ishii, Akinori Takami, Seiji Sugata, and Tatsuya Nagashima of University of Tsukuba, Coorporative Graduate School Program and Dr. Akio Yamagami of MRI, Dr. Joseph Ching of University of Tottori, Mr. Tomoki Kajikawa, Ms. Rio Ishikawa, and Mr. Takuya Nakagawa of University of Tsukuba for useful discussion and comments on this study. This research was supported by Japanese Society for the Promotion of Sciences (JSPS) Grant-in-Aid for JSPS Fellows Grant Nos. JP21J22912 and Environmental Research and Technology Development Fund of the Environmental Restoration and Conservation Agency (ERCA) (JPMEERF20215003).

Conflict of interest

The authors declare no conflicts of interest relevant to this study.

Data availability statement

The raw data of REASv3.2.1 can be obtained from https://www.nies.go.jp/REAS/ (last accessed: July 07, 2022). The screened data of AEROS are available at https://soramame.env.go.jp/download (last accessed: 7 July 2022).

References

Amann, M., Derwent, D., Forsberg, B., Hänninen, O., Hurley, F., Krzyzanowski, M., Frank de Leeuw, Liu, S., Mandin, C., Schneider, J., Schwarze, P. and Simpson, D., (2008). Health risks of ozone from long-range transboundary air pollution. World Health Organization. Regional Office for Europe. https://apps.who.int/iris/handle/10665/326496

Atkinson, R. (1994). Gas-phase tropospheric chemistry of organic compounds. *Journal of Physical and Chemical Reference Data.* 2, 1-216

630 Atkinson, R. (1997). Gas-phase tropospheric chemistry of volatile organic compounds: 1.
631 Alkanes and alkenes. *Journal of Physical and Chemical Reference Data,* 26(2), 215–290.
632 https://doi.org/10.1063/1.556012

633 Atkinson, R. (2000). Atmospheric chemistry of VOCs and NO_x. *Atmospheric Environment,* 34,
634 2063–2101.

635 Carter, W. P. L. (1994). Development of ozone reactivity scales for volatile organic compounds.
636 *Journal of the Air and Waste Management Association*, 44(7), 881–899.
637 https://doi.org/10.1080/1073161x.1994.10467290

638 Carter, W. P. L. (2000). Documentation of the SAPRC-99 Chemical Mechanism for VOC
639 Reactivity Assessment. Report to the California Air Resources Board, Contract 92-329
640 and 95-308.

641 Central Environmental Council, (2017), Future Policy for Motor Vehicle Emission Reduction
642 (Thirteenth Report), https://www.env.go.jp/air/car/taisaku/index.html (last accessed: 1
643 July 2022) (in Japanese)

644 Central Environmental Council, (2022), Future Policy for Motor Vehicle Emission Reduction
645 (Fourteenth Report), https://www.env.go.jp/air/car/taisaku/index.html (last accessed: 1
646 July 2022) (in Japanese)

647 Enami, S., Hoffmann, M. R. and Colussi, A. J. (2008). Acidity enhances the formation of a
648 persistent ozonide at aqueous ascorbate/ozone gas interfaces. *PNAS,* 105 (21), 7365–7369.
649 www.pnas.org/cgi/content/full/

650 Fukui, T., Kokuryo, K., Baba, T. and Kannari, A. (2014). Updating EAGrid2000‐Japan
651 emissions inventory based on the recent emission trends. *Journal of Japan Society for*
652 *Atmospheric Environment*, 49(2), 117–125. (in Japanese)

653 Giglio, L., Randerson, J.T. and Van Der Werf, G.R. (2013). Analysis of daily, monthly, and
654 annual burned area using the fourth-generation global fire emissions database (GFED4).
655 Journal of Geophysical Research: Biogeosciences, 118, 317–328.

656 Guenther, A., Karl, T., Harley, P., Wiedinmyer, C., Palmer, P. I. and Geron, C. (2006). Estimates
657 of global terrestrial isoprene emissions using MEGAN (Model of Emissions of Gases and

Aerosols from Nature). *Atmospheric Chemistry and Physics* (Vol. 6). www.atmos-chem-phys.net/6/3181/2006/

Hagino, H., Morikawa, T., Akiyama, K. and Sasaki, S. (2015). Volatile Organic Compounds and Air Quality Assessment Using Ozone Formation Potential in Refueling Loss Tests and Diurnal Breathing Loss Tests Using a Gasoline Fuel with Low Olefins. *Journal of Japan Society for Atmospheric Environment* (Vol. 50, Issue 6). (in Japanese)

Hata, H. and Tonokura, K. (2019). Impact of next-generation vehicles on tropospheric ozone estimated by chemical transport model in the Kanto region of Japan. *Scientific Reports,* 9(1). https://doi.org/10.1038/s41598-019-40012-y

Inoue, K., Yasuda, R., Yoshikado, H. and Higashino, H. (2010a). Spatial distribution of summer-time surface ozone sensitivity to NO_x and VOC emissions for the Kanto area Part 1: Estimation by numerical simulations with two kinds of (larger and smaller) biogenic emission estimates. *Journal of Japan Society for Atmospheric Environment,* 45 (5). 183–194. (in Japanese)

Inoue, K., Yoshikado, H. and Higashino, H. (2010b). Spatial distribution of summer-time surface ozone sensitivity to NO_x and VOC emissions for the Kanto area Part2: Estimation based on the measurement of a photochemical indicator. *Journal of Japan Society for Atmospheric Environment,* 45 (5). 195–204. (in Japanese)

Ito, A., Wakamatsu, S., Morikawa, T. and Kobayashi, S. (2021). 30 years of air quality trends in Japan. *Atmosphere,* 12(8). https://doi.org/10.3390/atmos12081072

Kajino, M., Deushi, M., Sekiyama, T. T., Oshima, N., Yumimoto, K., Tanaka, T. Y., Ching, J., Hashimoto, A., Yamamoto, T., Ikegami, M., Kamada, A., Miyashita, M., Inomata, Y., Shima, S. I., Takami, A., Shimizu, A. and Hatakeyama, S. (2019). NHM-Chem, the Japan meteorological agency's regional meteorology – chemistry model: Model evaluations toward the consistent predictions of the chemical, physical, and optical properties of aerosols. *Journal of the Meteorological Society of Japan,* 97(2), 337–374. https://doi.org/10.2151/JMSJ.2019-020

Kajino, M., Deushi, M., Sekiyama, T. T., Oshima, N., Yumimoto, K., Tanaka, T. Y., Ching, J., Hashimoto, A., Yamamoto, T., Ikegami, M., Kamada, A., Miyashita, M., Inomata, Y.,

687 Shima, S.-I., Khatri, P., Shimizu, A., Irie, H., Adachi, K., Zaizen, Y. and Mikami, M.
688 (2021). Comparison of three aerosol representations of NHM-Chem (v1.0) for the
689 simulations of air quality and climate-relevant variables. *Geosci. Model Dev.,* 14, 2235-
690 2264, https://doi.org/10.5194/gmd-14-2235-2021

691 Kannari, A., Tonooka, Y., Baba, T. and Murano, K. (2007). Development of multiple-species 1
692 km × 1 km resolution hourly basis emissions inventory for Japan. *Atmospheric*
693 *Environment,* 41(16), 3428–3439. https://doi.org/10.1016/j.atmosenv.2006.12.015

694 Kannari, A. and Ohara, T. (2010). Theoretical implication of reversals of the ozone weekend
695 effect systematically observed in Japan. *Atmospheric Chemistry and Physics*, 10, 6765–
696 6776

697 Ke, W., Zhang, S., Wu, Y., Zhao, B., Wang, S. and Hao, J. (2016). Assessing the future vehicle
698 fleet electrification: The impacts on regional and Urban air quality. *Environmental*
699 *Science and Technology,* 51(2), 1007–1016. https://doi.org/10.1021/acs.est.6b04253

700 Kleinman, L. I. (1994). Low and high NO_x tropospheric photochemistry. *Journal of Geophysical*
701 *Research*, Vol. 99, Issue D8.

702 Kobayashi, S., Ota, Y., Harada, Y., Ebita, A., Moriya, M., Onoda, H., Onogi, K., Kamahori, H.,
703 Kobayashi, C., Endo, H., Miyaoka, K. and Kiyotoshi, T. (2015). The JRA-55 reanalysis:
704 General specifications and basic characteristics. *Journal of the Meteorological Society of*
705 *Japan,* 93(1), 5–48. https://doi.org/10.2151/jmsj.2015-001

706 Kurokawa, J. and Ohara, T. (2020). Long-term historical trends in air pollutant emissions in
707 Asia: Regional Emission inventory in ASia (REAS) version 3. *Atmospheric Chemistry*
708 *and Physics,* 20(21), 12761–12793. https://doi.org/10.5194/acp-20-12761-2020

709 Lei, W., Foy, B., Zavala, M., Volkamer, R. and Molina, L. T. (2007). Characterizing ozone
710 production in the Mexico City Metropolitan Area: a case study using a chemical transport
711 model, *Atmospheric Chemistry and Physics*, 7, 1347–1366

712 Li, N., Chen, J. P., Tsai, I. C., He, Q., Chi, S. Y., Lin, Y. C. and Fu, T. M. (2016). Potential
713 impacts of electric vehicles on air quality in Taiwan. *Science of the Total Environment,*
714 566–567, 919–928. https://doi.org/10.1016/j.scitotenv.2016.05.105

715 Martilli, A., Neftel, A., Favaro, G., Kirchner, F., Sillman, S. and Clappier, A. (2002). Simulation
716 of the ozone formation in the northern part of the Po Valley. *Journal of Geophysical*
717 *Research*, 107(D22), 8195. https://doi.org/10.1029/2001JD000534ï

718 Milford, J. B., Russell, A. G. and McRae, G. J., (1989). A New Approach to Photochemical
719 Pollution Control: Implications of Spatial Patterns in Pollutant Responses to Reductions
720 in Nitrogen Oxides and Reactive Organic Gas Emissions. *Environ. Sci. Technol.* 1989, 23,
721 1290-1301

722 Ministry of Land, Infrastructure and Transport, (2010), National Road and Street Traffic
723 Conditions Survey (Road Traffic Census), https://www.mlit.go.jp/road/census/h22-1/,
724 (last accessed: 5 July 2022) (in Japanese)

725 Ministry of Land, Infrastructure and Transport, urban bureau, (2012), Guidelines for the
726 Installation of Charging Facilities in Parking Lots, etc. Guidelines for the Installation of
727 Charging Facilities in Parking Lots, etc., https://www.mlit.go.jp/common/000212869.pdf,
728 (last accessed: 5 July 2022) (in Japanese)

729 Ministry of Land, Infrastructure and Transport, (2012), Annual Report on Fuel Consumption of
730 Automobiles. https://www.mlit.go.jp/k-
731 toukei/22/errata/kaitei/annual/pdf/new/22201200a00000_n.pdf, (last accessed: 5 July
732 2022) (in Japanese)

733 Morikawa, T. (2017). Current status of Japanese emission inventory for PM2.5 and its problems.
734 *Journal of Japan Society for Atmospheric Environment*, 52(3), A74–A78. (in Japanese)

735 Nakagawa, Y., Inoue, K., Yamada, H. and Tonokura, K. (2019). Assessment of Reduction of
736 Fuel Evaporative Emission at the Time of Refueling on Air Quality in the Kanto Region,
737 *Transactions of Society of Automotive Engineers of Japan,* 50(5) 1458-1462 (in Japanese).

738 Nopmongcol, U., Grant, J., Knipping, E., Alexander, M., Schurhoff, R., Young, D., Jung, J.,
739 Shah, T. and Yarwood, G. (2017). Air Quality Impacts of Electrifying Vehicles and
740 Equipment Across the United States. *Environmental Science and Technology*, 51(5),
741 2830–2837. https://doi.org/10.1021/acs.est.6b04868

742 Ooka, R., Khiem, M., Hayami, H., Yoshikado, H., Huang, H. and Kawamoto, Y. (2011).
743 Influence of meteorological conditions on summer ozone levels in the central Kanto area

744 of Japan. *Procedia Environmental Sciences*, 4, 138–150.
745 https://doi.org/10.1016/j.proenv.2011.03.017

746 Pan, S., Roy, A., Choi, Y., Eslami, E., Thomas, S., Jiang, X. and Gao, H. O. (2019). Potential
747 impacts of electric vehicles on air quality and health endpoints in the Greater Houston
748 Area in 2040. *Atmospheric Environment,* 207, 38–51.
749 https://doi.org/10.1016/j.atmosenv.2019.03.022

750 Schnell, J. L., Naik, V., Horowitz, L. W., Paulot, F., Ginoux, P., Zhao, M., & Horton, D. E.
751 (2019). Air quality impacts from the electrification of light-duty passenger vehicles in the
752 United States. *Atmospheric Environment,* 208, 95–102.
753 https://doi.org/10.1016/j.atmosenv.2019.04.003

754 Schraufnagel, D. E., Balmes, J. R., Cowl, C. T., de Matteis, S., Jung, S. H., Mortimer, K., Perez-
755 Padilla, R., Rice, M. B., Riojas-Rodriguez, H., Sood, A., Thurston, G. D., To, T., Vanker,
756 A., & Wuebbles, D. J. (2019). Air Pollution and Noncommunicable Diseases: A Review
757 by the Forum of International Respiratory Societies' Environmental Committee, Part 1:
758 The Damaging Effects of Air Pollution. *Chest,* 155(2), 409–416. Elsevier Inc.
759 https://doi.org/10.1016/j.chest.2018.10.042

760 Sillman, S. (1995). The use of NO_y, H_2O_2, and HNO_3 as indicators for ozone- NO_x-hydrocarbon
761 sensitivity in urban locations. *Journal of Geophysycal Research*, 100(D7), 14,175-14,188.

762 Sillman, S. (1999). The relation between ozone, NO_x and hydrocarbons in urban and polluted
763 rural environments. *Atmospheric Environment* (Vol. 33).

764 Sillman, S. and He, D. (2002). Some theoretical results concerning O_3-NO_x-VOC chemistry and
765 NO_x-VOC indicators. *Journal of Geophysical Research Atmospheres,* 107(22).
766 https://doi.org/10.1029/2001JD001123

767 Song, J., Lei, W., Bei, N., Zavala, M., de Foy, B., Volkamer, R., Cardenas, B., Zheng, J., Zhang,
768 R. and Molina, L. T. (2010). Ozone response to emission changes: a modeling study
769 during the MCMA-2006/MILAGRO Campaign. *Atmospheric Chemistry and Physics*,
770 (Vol. 10). www.atmos-chem-phys.net/10/3827/2010/

771 Soret, A., Guevara, M. and Baldasano, J. M. (2014). The potential impacts of electric vehicles on
772 air quality in the urban areas of Barcelona and Madrid (Spain). *Atmospheric Environment,*
773 99, 51–63. https://doi.org/10.1016/j.atmosenv.2014.09.048

774 Spirig, C., Neftel, A., Kleinman, L. I. and Hjorth, J. (2002). NO_x versus VOC limitation of O_3
775 production in the Po valley: Local and integrated view based on observations. *Journal of*
776 *Geophysical Research: Atmospheres,* 107(22). https://doi.org/10.1029/2001JD000561

777 Tager, I. B., Balmes, J., Lurmann, F., Ngo, L., Alcorn, S. and Künzli, N. (2005). Chronic
778 exposure to ambient ozone and lung function in young adults. *Epidemiology*, 16(6), 751–
779 759. https://doi.org/10.1097/01.ede.0000183166.68809.b0

780 Tajima, Y., Kato, S., Suthawaree, J. and Kajii, Y. (2010). Long-term measurement of various
781 volatile organic compounds and air quality assessment using OH reactivity and ozone
782 formation potential in sub-urban area of Tokyo. *Journal of Japan Society for*
783 *Atmospheric Environment,* 45(2), 56–65.

784 Tang, Y., Dong, Y., Wittlin, S., Charman, S. A., Chollet, J., Chiu, F. C. K., Charman, W. N.,
785 Matile, H., Urwyler, H., Dorn, A., Bajpai, S., Wang, X., Padmanilayam, M., Karle, J. M.,
786 Brun, R. and Vennerstrom, J. L. (2007). Weak base dispiro-1,2,4-trioxolanes: Potent
787 antimalarial ozonides. *Bioorganic and Medicinal Chemistry Letters,* 17(5), 1260–1265.
788 https://doi.org/10.1016/j.bmcl.2006.12.007

789 Thompson, T., Webber, M. and Allen, D. T. (2009). Air quality impacts of using overnight
790 electricity generation to charge plug-in hybrid electric vehicles for daytime use.
791 *Environmental Research Letters,* 4(1). https://doi.org/10.1088/1748-9326/4/1/014002

792 Thompson, M. T., King, C. W., Allen, D. T. and Webber, M. E. (2011). Air quality impacts of
793 plug-in hybrid electric vehicles in Texas: Evaluating three battery charging scenarios.
794 *Environmental Research Letters,* 6(2). https://doi.org/10.1088/1748-9326/6/2/024004

795 Tonokura, K. and Hata, H (2020). Estimation of Evaporative Emissions from Parking
796 and Refueling Processes of Gasoline Vehicles, *Journal of Japan Society for Atmospheric*
797 *Environment,* 55(1), A1-A7

798 Uchida, R. (2016). Evaporative Emissions from Gasoline Vehicles-Review of Estimation for
799 Evaporative Emissions in the United State. *JARI Research Journal*, 20160902 (in
800 Japanese)

801 Uchida, Y., Ishii, K., Ueno, H., Yokota, H., & Akiyama, K. (2013). An Emission Characteristics
802 Study of Volatile Organic Compounds, Nitrogen Oxides and Fine Particulate Matter (PM
803 2.5) from Motor-Vehicles in a Road Tunnel in 2010: Comparison with 2001. *J. Jpn. Soc.*
804 *Atmos. Environ,* 48 (3), 145–153(in Japanese)

805 Vermeuel, M. P., Novak, G. A., Alwe, H. D., Hughes, D. D., Kaleel, R., Dickens, A. F., Kenski,
806 D., Czarnetzki, A. C., Stone, E. A., Stanier, C. O., Pierce, R. B., Millet, D. B. and
807 Bertram, T. H. (2019). Sensitivity of Ozone Production to NO_x and VOC Along the Lake
808 Michigan Coastline. *Journal of Geophysical Research: Atmospheres,* 124(20), 10989–
809 11006. https://doi.org/10.1029/2019JD030842

810 Yamada, H., Inomata, S. and Tanimoto, H. (2015a). Evaporative emissions in three-day diurnal
811 breathing loss tests on passenger cars for the Japanese market. *Atmospheric Environment,*
812 107, 166–173. https://doi.org/10.1016/j.atmosenv.2015.02.032

813 Yamada, H., Inomata, S. and Tanimoto, H. (2015b). Refueling emissions from cars in Japan:
814 Compositions, temperature dependence and effect of vapor liquefied collection system.
815 *Atmospheric Environment,* 120, 455–462.
816 https://doi.org/10.1016/j.atmosenv.2015.09.026

817 Zhang, J.J., Wei, Y. and Fang, Z. (2019). Ozone Pollution: A Major Health Hazard Worldwide.
818 *Frontiers in Immunology*, 10, 2518.

819

820 **References from Supporting Information**

821 Clarke, A. D., Owens, S. R. and Zhou, J. (2006). An ultrafine sea-salt flux from breaking waves:
822 Implications for cloud condensation nuclei in the remote marine atmosphere. *Journal of*
823 *Geophysical Research*, 111, D06202, 14 pp.

824 Deushi, M. and Shibata, K. (2011). Development of an MRI Chemistry-Climate Model ver.2 for
825 the study of tropospheric and stratospheric chemistry. *Papers in Meteorology and*
826 *Geophysics*, 62, 1-46.

827 Han, Z., Ueda, H., Matsuda, K., Zhang, R., Arao, K., Kanai, Y. and Hasome, H. (2004). Model
828 study on particle size segregation and deposition during Asian dust events in March 2002.
829 *Journal of Geophysical Research*, 109, D19205, 22 pp.

830 Tanaka, T., Y., Orito, K., Sekiyama, T. T., Shibata, K., Chiba, M. and Tanaka, H. (2003).
831 MASINGAR, a global tropospheric aerosol chemical transport model coupled with
832 MRI/JMA98 GCM: Model description. *Papers in Meteorology and Geophysics*, 53(4),
833 119-138.

834 Tanaka, T. Y. and Ogi, A. (2017). Update of Japan Meteorological Agency's global mineral dust
835 operational forecast model. Sokkou-Jihou, 84, 109-128 (in Japanese).

836 Yumimoto, K., Tanaka, T., Y., Oshima, N. and Maki, T. (2017). JRAero: the Japanese
837 Reanalysis for Aerosol v1.0. *Geoscientific Model Development,* 10, 3225-3253.

838

839

840

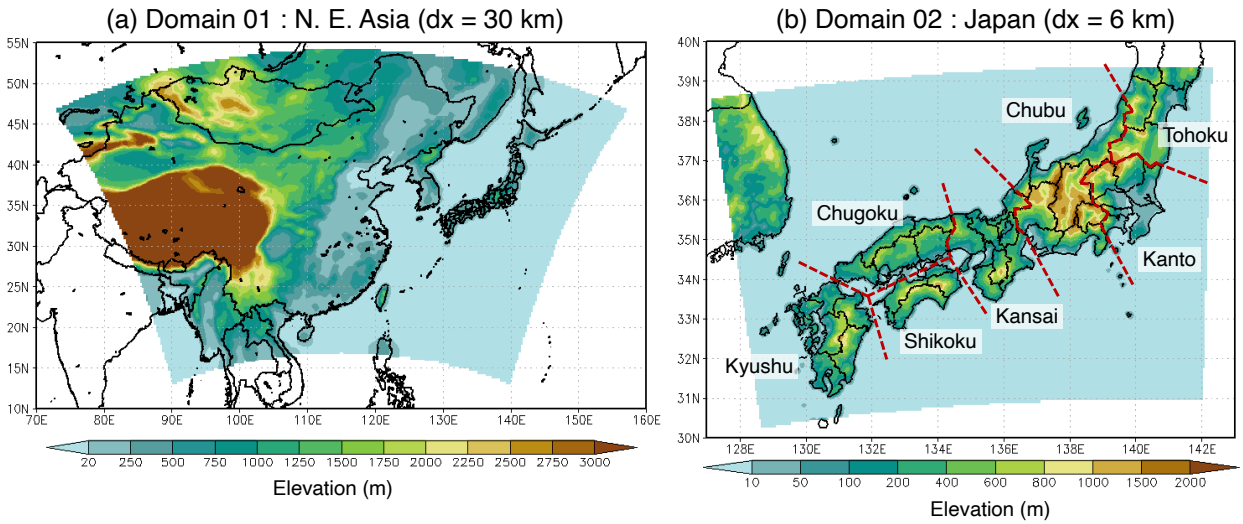

841

842 **Figure 1.** Model domains in this study. (a) Terrestrial elevations of domain 01 (North East Asia,
843 dx = 30 km). (b) Same as (a) but for domain 02 (Japan, dx = 6 km).

844

845

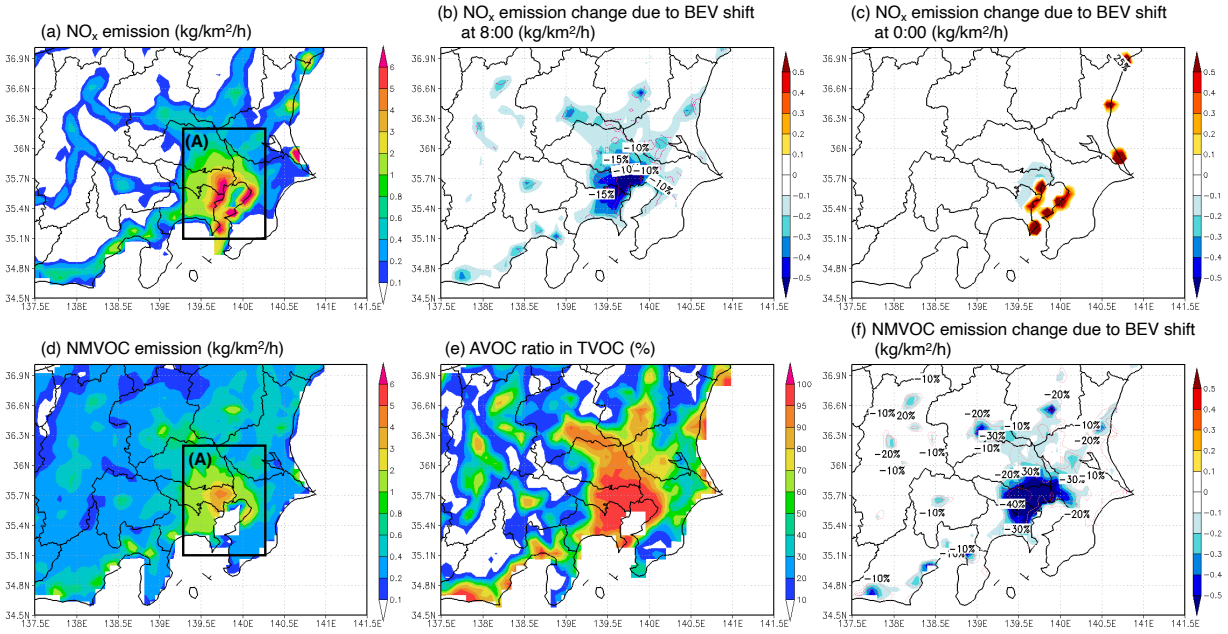

Figure 2. Monthly mean NO_x and NMVOC emissions in the BASE experiment and their changes in all BEV experiments in Kanto in July 2015: (a) NO_x emission flux in the BASE experiment, (b) changes in NO_x flux at 8:00 a.m. local time, (c) changes in NO_x flux at 0:00 a.m. local time, (d) NMVOC emission flux in the BASE experiment, (e) anthropogenic ratio to the total NMVOC emission flux in the BASE experiment, and (f) changes in NMVOC flux due to BEV shift. The major emission source area is framed (A).

854

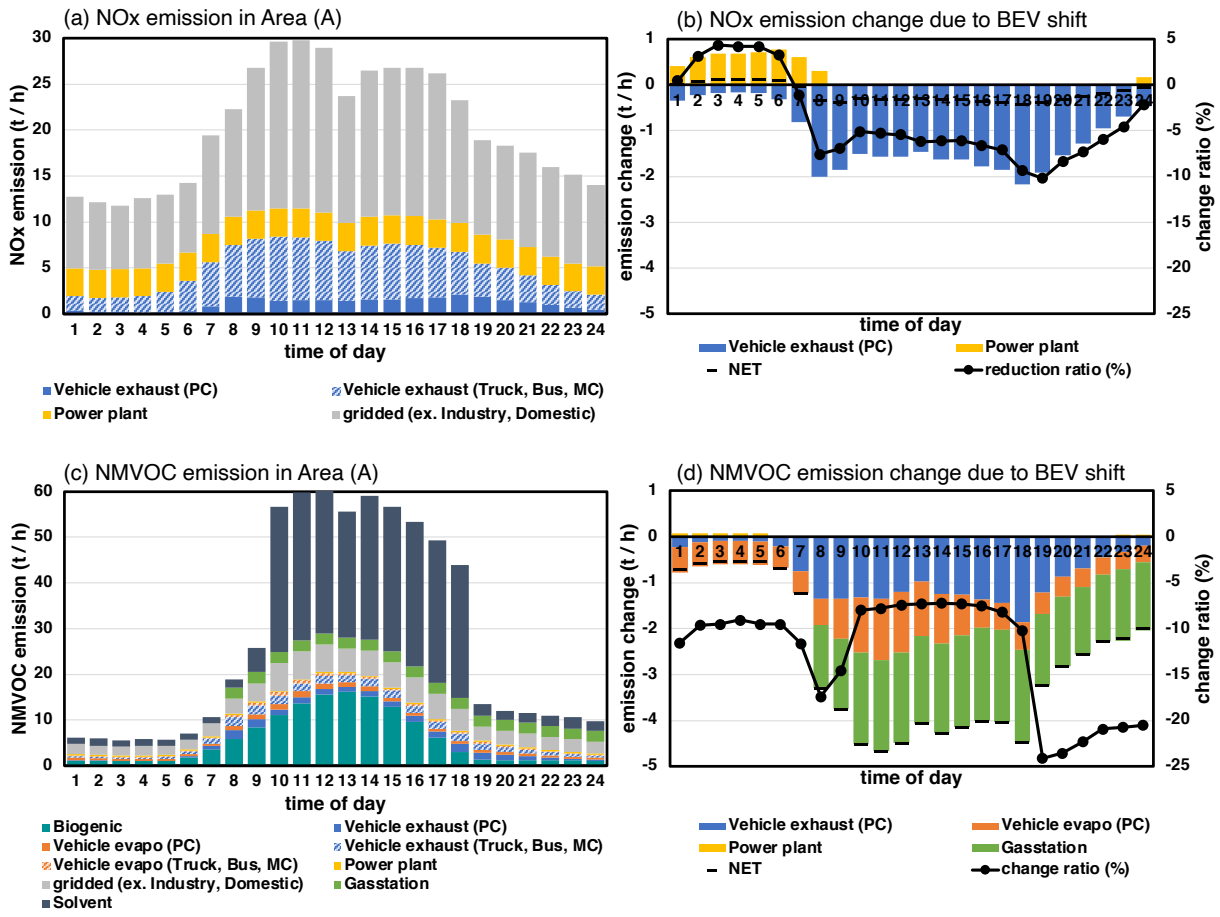

855

856 **Figure 3.** Diurnal variation of the monthly and areal mean (a) NOx and (b) NMVOC emissions
857 and (c, d) their emission changes in all BEV experiments in the area (A) (Figure 2). Weekdays
858 and weekends are weighted by the number of days in July.

859

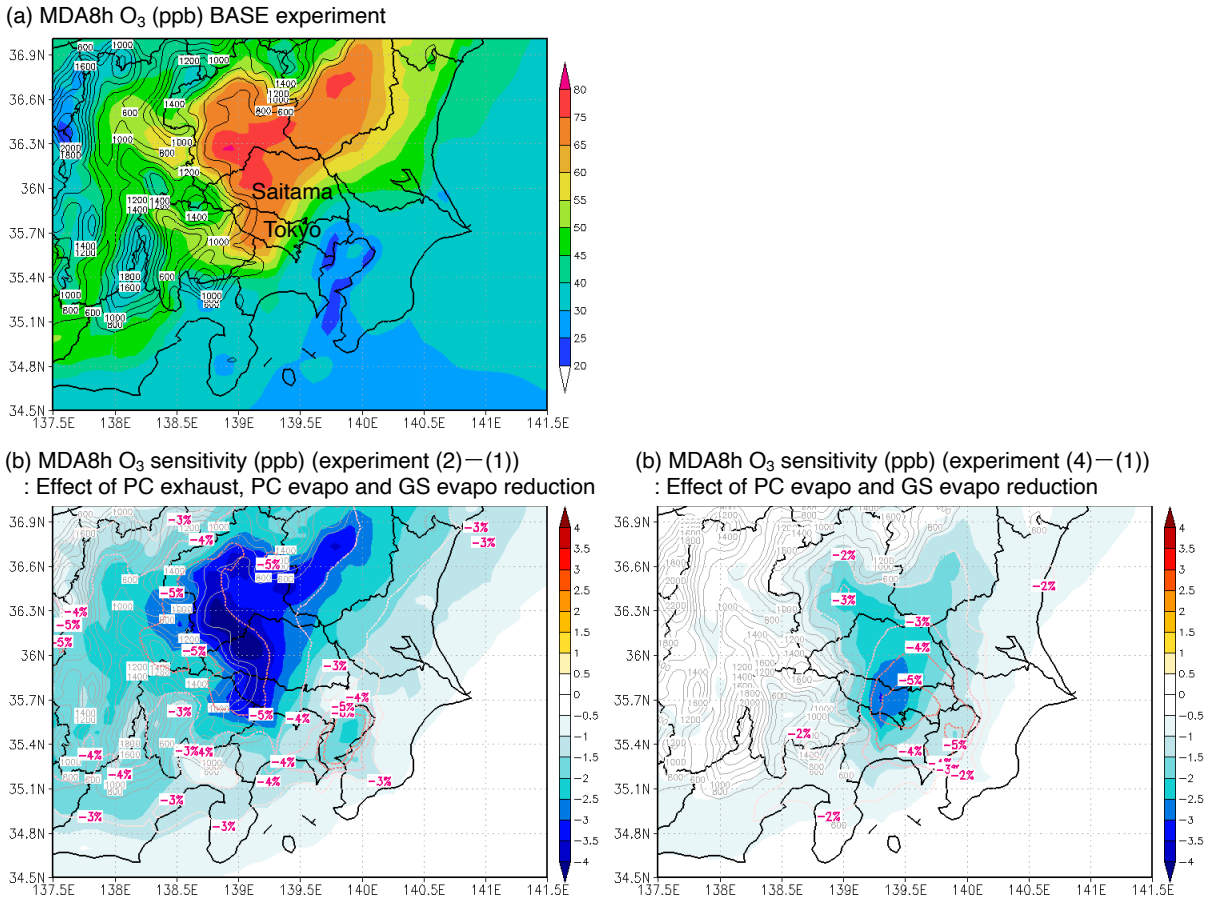

Figure 4. Monthly mean concentrations of MDA8h O_3 in July 2015: (a) BASE experimental result, (b) sensitivity of all BEV experiment, and (c) sensitivity of Evapo reduction experiment (c), respectively. Numbers in the title of each panel correspond to the sensitivity experiment, as listed in Table 1. The thin black or gray contours indicate terrestrial elevation (m). The pink contours of (b) and (c) indicate the change ratio of O_3 concentration (%).

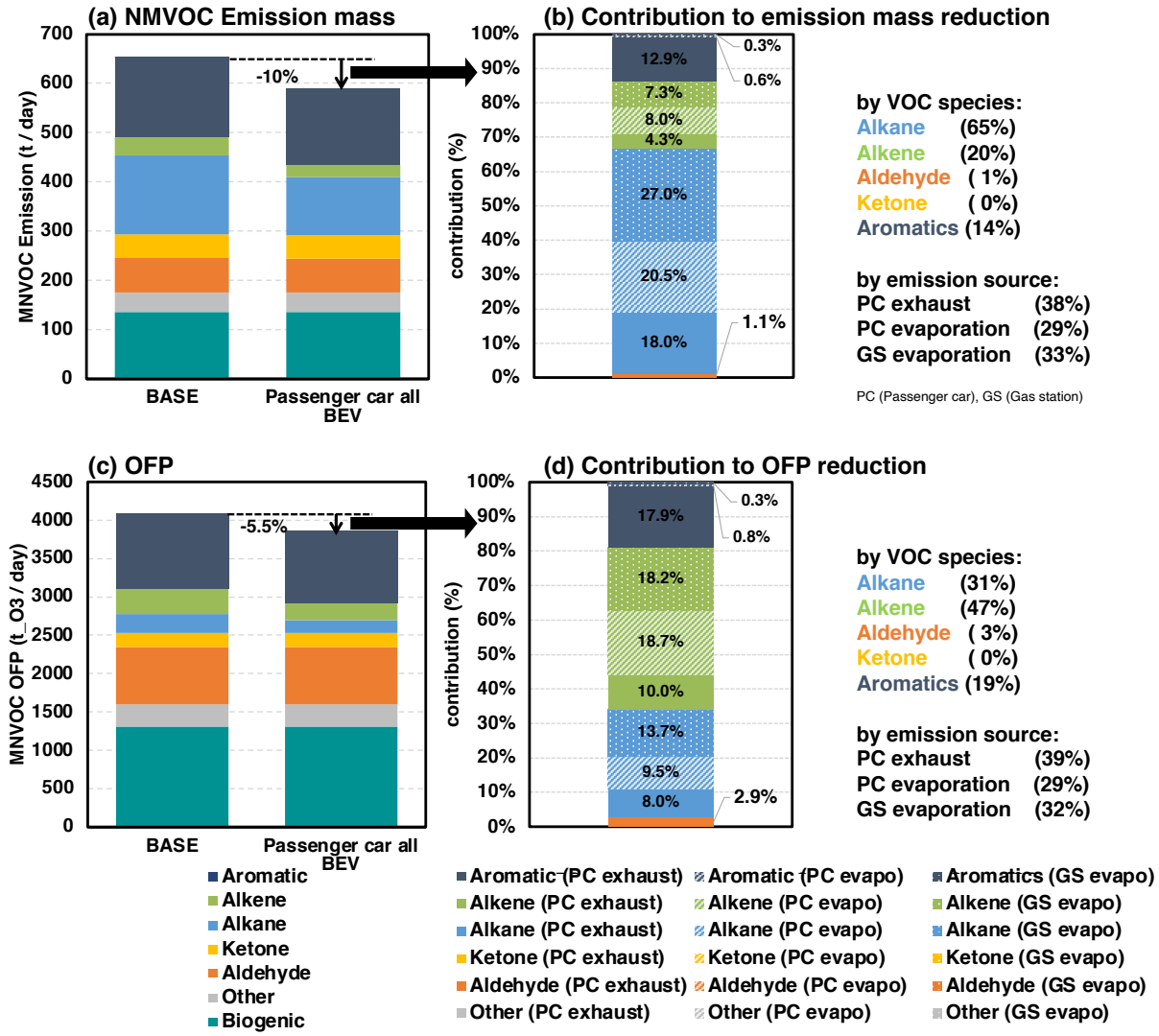

867

868 **Figure 5.** Monthly and areal total emissions of NMVOC (a) mass and (c) ozone formation
869 potential (OFP) with the contributions of VOC speciation in the BASE experiment and their
870 changes in all BEV experiments in the area (A) (Figure 2). 5b and 5d show the contribution of
871 each VOC specie and emission source to the reductions of 5a and 5c, respectively. OFP is
872 NMVOC emissions weighted by maximum incremental reactivity (MIR). The values of MIR
873 based on the SAPRC-99 speciation (*Carter,* 2000) are shown in Table S2.

874

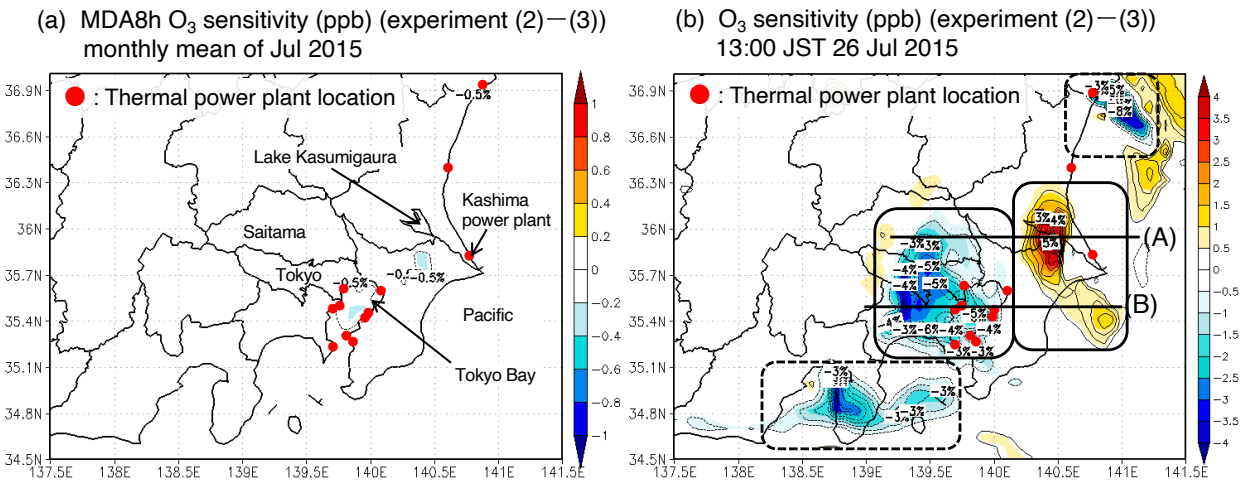

875

876 **Figure 6.** The sensitivity of the next daytime O_3 concentration is due to additional thermal power
877 plant emission for BEV night charging. MDA8h O_3 of July average (a) and the case of 14:00 JST
878 26 July (b). Numbers in the title of each panel correspond to the sensitivity experiment, as listed
879 in Table 1. Thermal power plant locations are indicated by red dots. (A) and (B) each passes
880 through a point of high sensitivity. In the region enclosed with the solid line (b), the positive and
881 negative sensitivity of O_3 is consistent with the general O_3 sensitivity regime (VOC-limited in
882 urban and NO_x-limited in the suburb). In the region enclosed with the dashed line (b), O_3
883 sensitivity is not consistent with the general sensitivity regime.

884

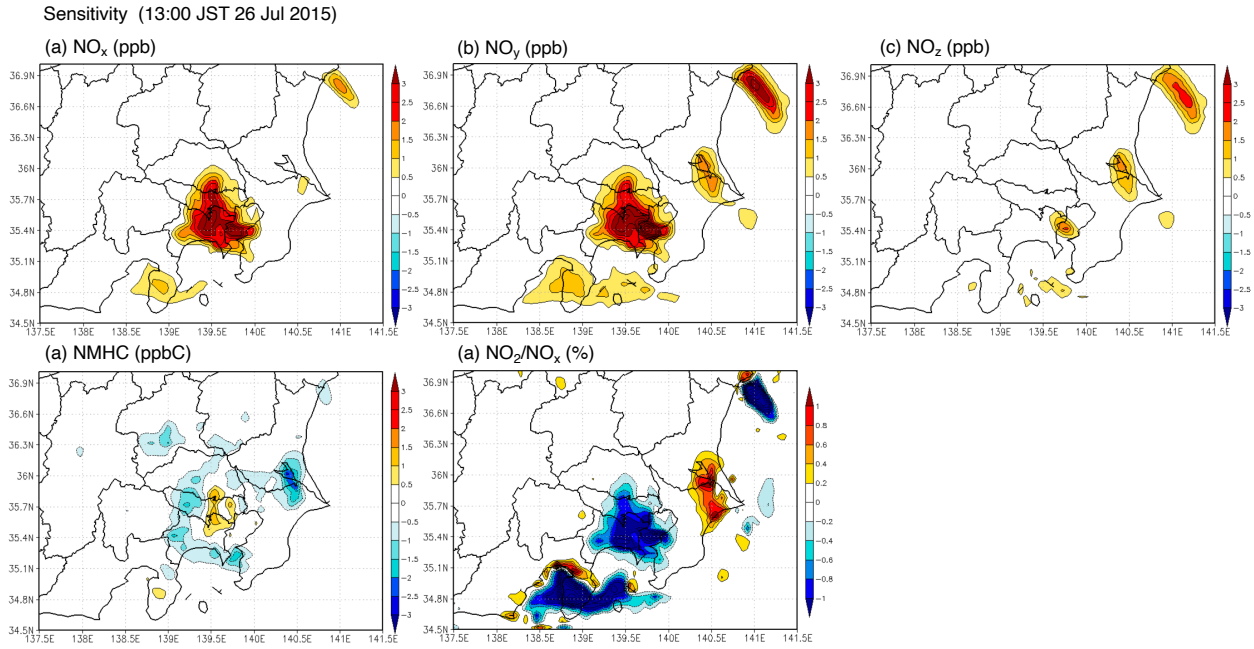

885

886 **Figure 7.** The sensitivity of next daytime NO_x, NO_y, NO_z, NMHC concentration, and NO_2/NO_x

887 ratio due to the additional thermal power plant emission for BEV night charging (the case of

888 14:00 JST 26 July).

889

890

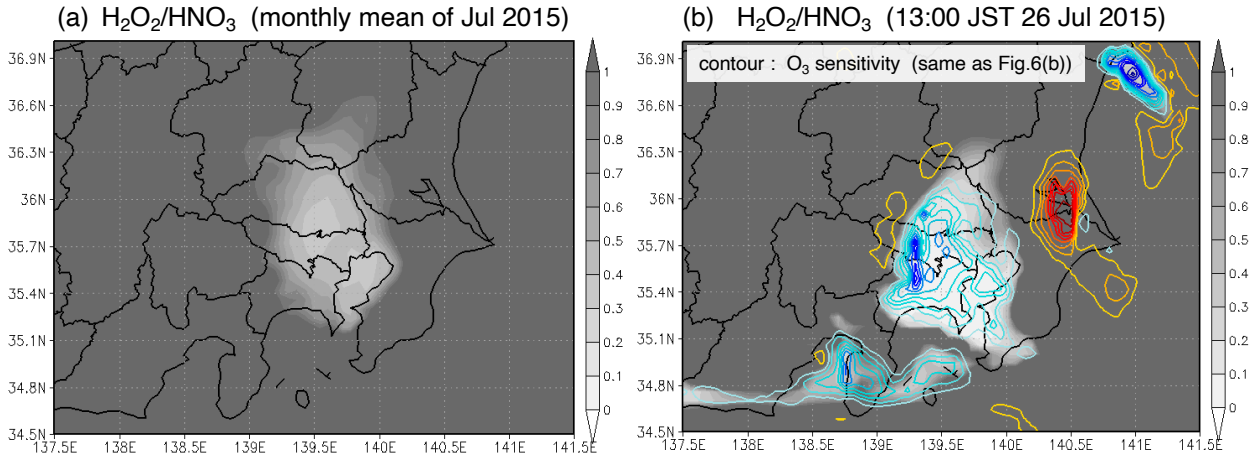

891

892 **Figure 8.** The distribution of H_2O_2/HNO_3. July average (a) and the case of 14:00 JST 26 July (b).

893 The contour of (b) indicates O_3 sensitivity, as shown in Figure 6b.

894

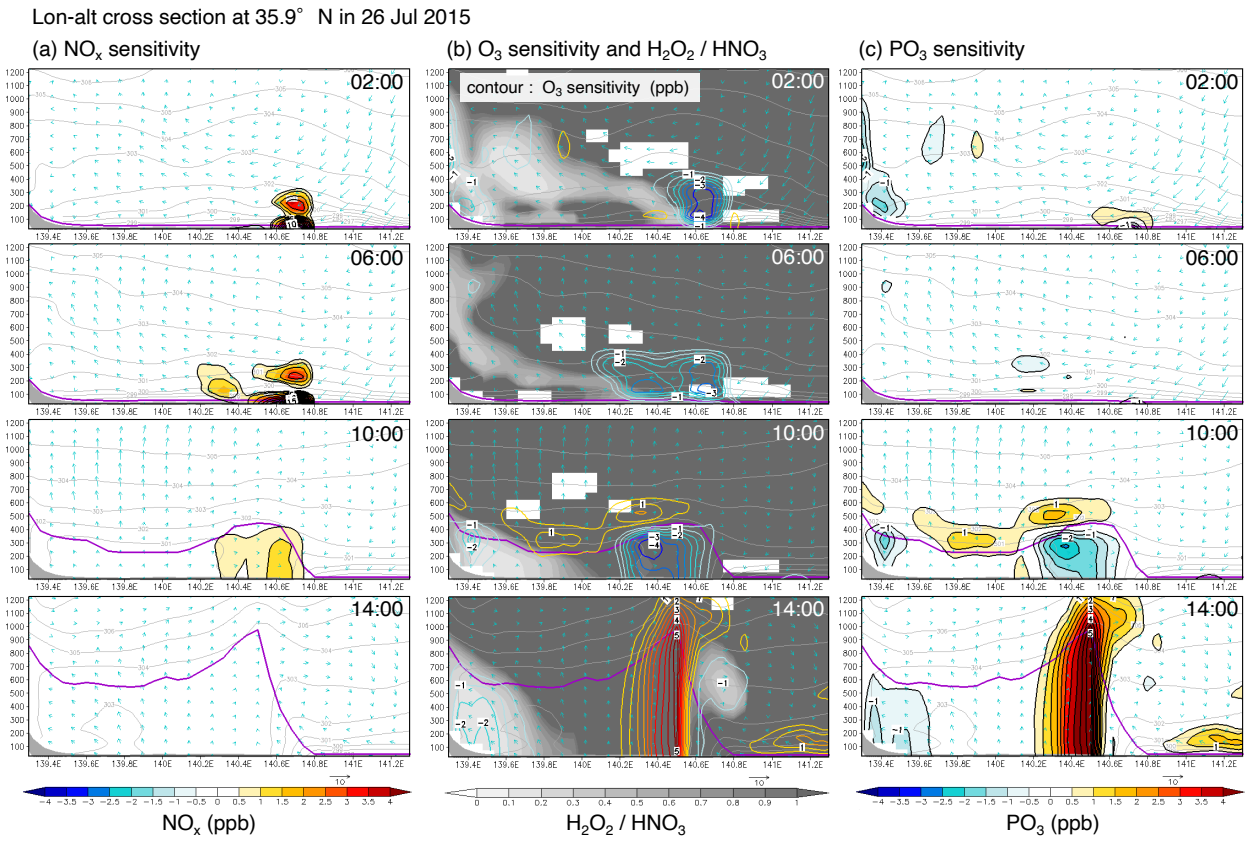

895

896 **Figure 9.** Longitude–altitude cross-section at 35.9°N shown in Figure 6b-line (A): (a) NO_x
897 sensitivity, (b) PO_3 sensitivity, and (c) O_3 sensitivity and H_2O_2/HNO_3, respectively. The Y-axis
898 indicates the height above sea level (m). The gray contours indicate the potential temperature.
899 The purple line indicates mixed layer altitude. The mixed layer altitude here is the lowest altitude
900 in the vertical profile of the virtual potential temperature of each layer of the model that exceeds
901 the virtual potential temperature of the lowest layer of the atmosphere. The H_2O_2/HNO_3 ratio has
902 an error value (infinity; white blank) when HNO_3 is extremely low in Figure 9b.

903

904

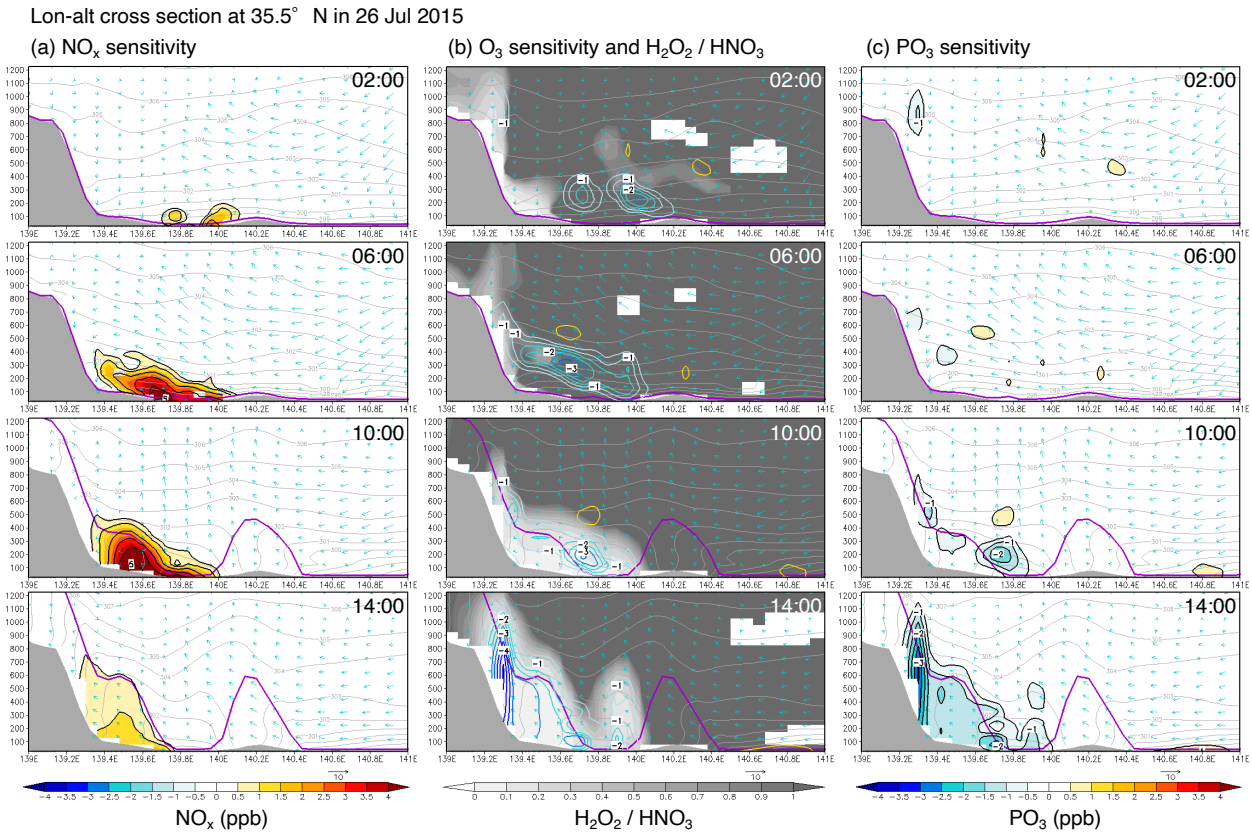

905

906 **Figure 10.** Same as Figure 9 but at 35.5°N shown in Figure 6b-line (B).

907

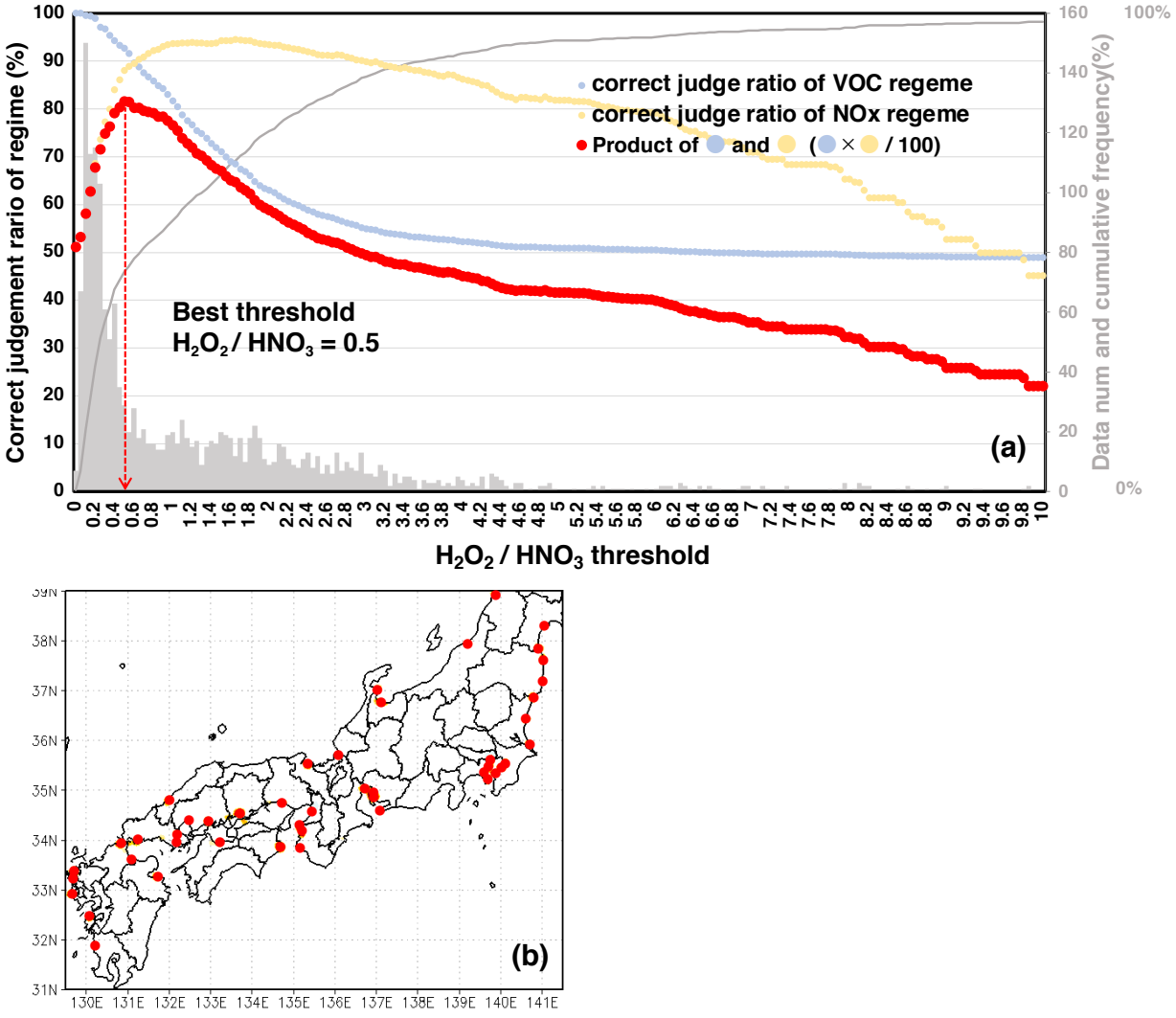

908

909 **Figure A1**. The correct judgment ratio of the O_3 sensitivity regime (NO_x- or VOC-limited) when
910 the H_2O_2/HNO_3 threshold is varied. The target is the grid data with $O_3 \geqq 70$ ppb and $|\Delta O_3| \geqq 0.5$
911 ppb from 10:00 to 15:00 on July 1 to 31 in the national area shown in (b). The histogram of
912 H_2O_2/HNO_3 corresponding to them is the right vertical axis in (a). In (a), the light blue graph
913 shows the percentage of negative O_3 sensitivity in the data with H_2O_2/HNO_3 below the threshold
914 (i.e., the percentage of the correct judgment of the VOC-limited). The light-yellow graph shows
915 the percentage of positive O_3 sensitivity in the data with H_2O_2/HNO_3 above the threshold (i.e.,
916 the percentage of the correct judgment of the NO_x-limited). The red graph is the product of light
917 blue and light-yellow.

918

Table 1. Simulation experimental cases in this study. Emission factors for the sensitivity experiments (2, 3, and 4) to base experiment (1) for each emission source of O_3 precursors.

Emission source	O_3 prediction	(1) BASE	(2) all BEV	(3) all BEV (PP[b] unchanged)	(4) Evapo reduce
Passenger car exhaust	NO_x, NMVOC, CO	1	0	0	1
Passenger car evaporation (RL, HSL, DBL)	NMVOC	1	0	0	0
Gas station evaporation	NMVOC	1	0.2	0.2	0.2
PP[b]	mainly NO_x	1	approximately 1.25[a] at 23:00~8:00	1	1

a. Reference Figure S1.

b. Thermal power plant.

925

926 **Table 2.** Statistical comparison of the model BASE experimental result and observation data for
927 O_3 and MDA8h O_3 in July 2015.

	Region	Period	N	Obs. mean	Sim. mean	R	MB	NMB (%)
O_3 (ppb)	Kanto (1 region)	July 2015 (31 days)	31	28.2	25.4	0.66	−2.7	−9.7
MDA8h O_3 (ppb)			31	44.8	46.4	0.79	1.6	3.6
O_3 (ppb)	Japan all (869 grid)	July 2015 (monthly mean)	869	24.6	25.5	0.32	0.9	3.8
MDA8h O_3 (ppb)			869	37.2	40.3	0.56	3.1	8.4

928

929

Journal of Geophysical Research: Atmosphere

Supporting Information for

Impact of battery electric vehicle penetration and corresponding changes in upstream processes on summer O_3 concentrations in Japan

Satoko Kayaba[1,2] and Mizuo Kajino[2,3]

1 Graduate School of Science and Technology, University of Tsukuba, Tsukuba, Ibaraki 305-8572, Japan

2 Meteorological Research Institute (MRI), Japan Meteorological Agency (JMA), Tsukuba, Ibaraki 305-0052, Japan

3 Faculty of Life and Environmental Sciences, University of Tsukuba, Tsukuba, Ibaraki 305-8572, Japan

Contents of this file

Introduction

This supporting information includes the following table and figures:

- Base and additional electricity demands for BEV charging (Fig. S1)
- Comparison of observation data and model simulation results with time series of hourly O_3 concentrations in Kanto in July 2015 (Fig. S2)
- VOC profiles of the exhaust (gasoline- and diesel-powered) and evaporation (HSR & RL, DBL, and gas station refueling) (Fig. S3)
- $(H_2O_2 + ROOH)/NO_z$ distributions (Fig. S4)
- The correct judgment ratio of the O_3 sensitivity regime (NO_x- or VOC-limited) when $(H_2O_2 + ROOH)/NO_z$ threshold is varied (Fig. S5)
- Details of the simulation setting in this study (Table. S1)
- List of MIR for the SUPRC-99 VOC group (Table. S2)

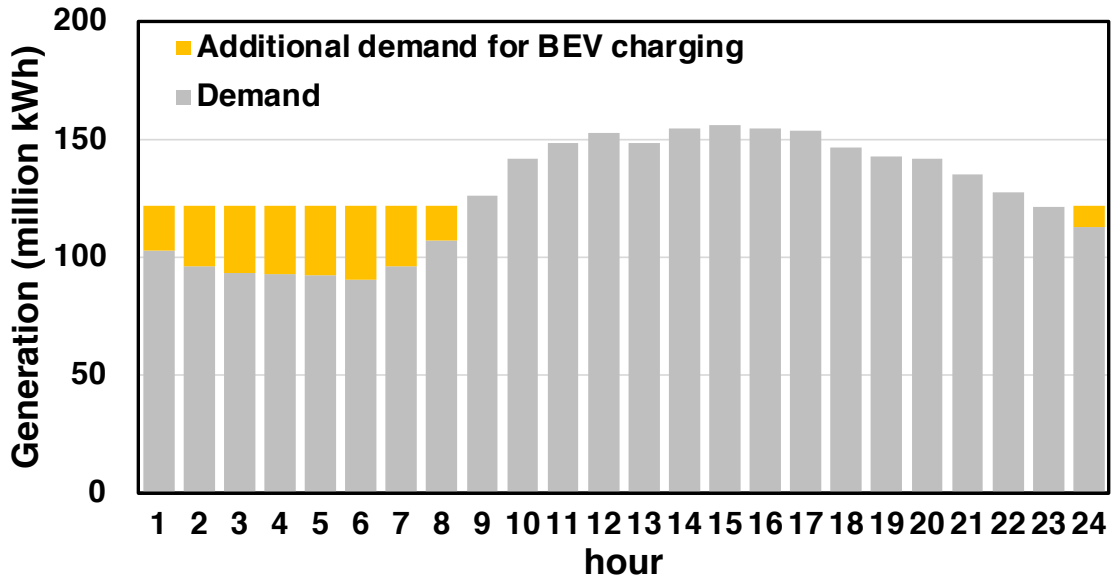

Figure S1. Additional electricity demand for BEV charging. The baseline demand is the demand pattern of July 27, 2012, which was used because the data were publicly available as electricity demand on the day of maximum electricity demand (according to the Power Companies of Japan: https://www.ene100.jp/zumen/1-2-10, last accessed: July 1, 2022). The additional demand was derived by the method in Section 2.2.2 of the main text.

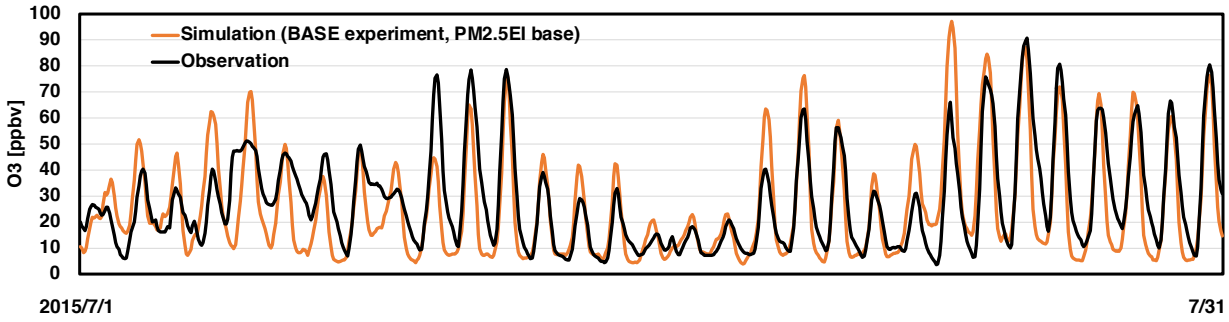

Figure S2. Time series of O_3 concentrations in Kanto in July 2015. Comparison of observation data (black line) and model simulation results (orange line).

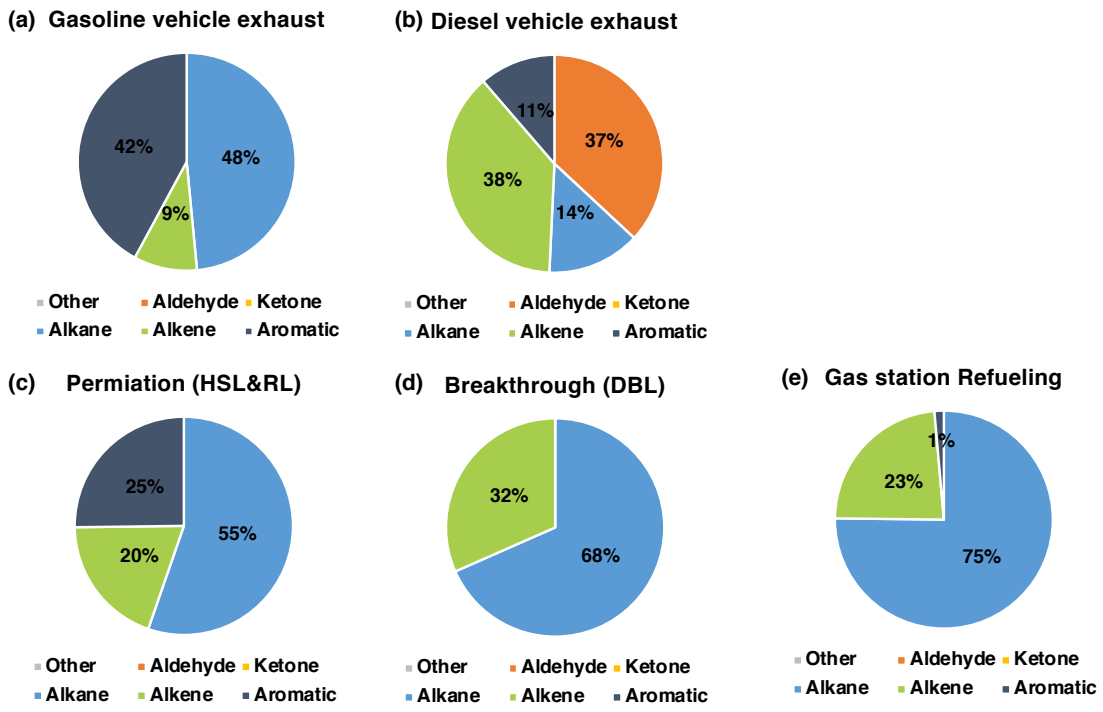

Figure S3. VOC profiles for each source. The components of exhaust gas in gasoline and diesel vehicles are the results of the tunnel survey by *Uchida et al.* (2013). The component of DBL is the result of the DBL test by *Yamada et al.* (2015a) after day 2 (caused by breakthrough). The component of HSL & RL is the result of the DBL test by *Yamada et al.* (2015a) on day 1 (caused by permeation). We determined that these data could be used because HSL & RL is mainly caused by the transmission. The component of refueling is the results of the test by *Yamada et al.* (2015b).

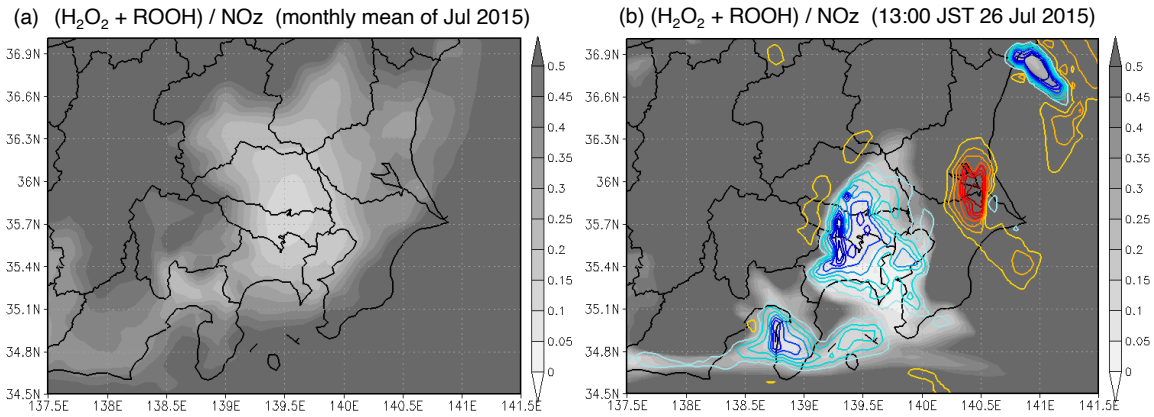

Figure S4. Same as Figure 8 but for (H_2O_2 + ROOH)/NOz.

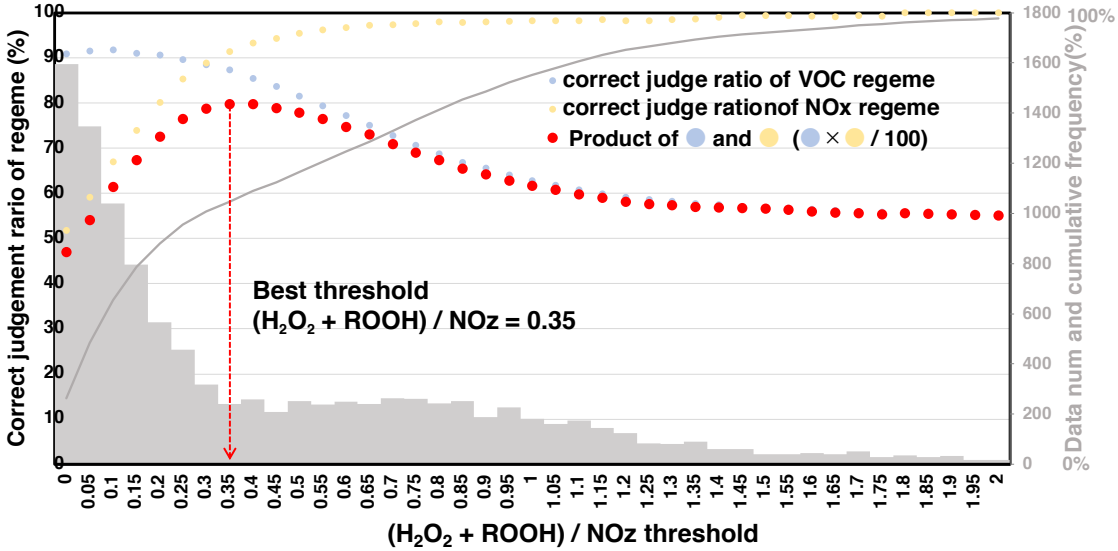

Figure S5. This is the same as Figure A1 but for (H_2O_2 + ROOH)/NOz.

Table S1. Simulation setting in this study

Model	Offline NHM-Chem[a] (*Kajino et al.,* 2019; *Kajino et al.,* 2021)	
Region	Domain 1: East Asia (dx = 30 km) Domain 2: Japan from Kyusyu to Tohoku (dx = 6 km)	
Period	From July 1 to 31, 2015	
Boundary conditions of NHM	Reanalysis data Domain 1: JRA-55, 6 hourly (*Kobayashi et al.,* 2015) Domain 2: JMA's Meso-Regional Objective Analysis (MA), 3 hourly (https://www.jma.go.jp/jma/jma-eng/jma-center/nwp/nwp-top.htm, last accessed: 30 July 2022).	
Boundary conditions of CTM[b]	Domain 1: monthly climatological data simulated by a global model Gases : MRI-CCM2 (*Deushi and Shibata,* 2011) Aerosols: MASINGAR-mk2 (*Tanaka et al.,* 2003; *Tanaka and Ogi,* 2017; *Yumimoto et al.,* 2017;) Domain 2: Domain 1	
Time intervals	1 h (output of NHM and input/output of CTM)	
Emission	Anthropogenic	East Asia: REASv3.2.1 (2015 base) (*Kurokawa and Ohara,* 2020) *REASv3.2.1 was updated from v3.2 in Dec 2021. Japan: PM2.5EI (2012 base) (*Morikawa,* 2017) + EAGrid for navigation (2010 base) (*Fukui et al.,* 2014; *Kannari et al.,* 2007)
	Biomass burning	GFED v4 (*Giglio et al.,* 2013)
	Biogenic VOC	MEGAN v2 (*Guenther et al.,* 2006)
	Volcano SO_2	Observation data of JMA
	Mineral dust	Inline calculation based on the method of *Han et al.* (2004)
	Sea salt	Inline calculation based on the method of *Clark et al.* (2006)

a. NHM-Chem is coupled with the meteorological model NHM offline or online. In the case of offline coupling, drive NHM first and then the chemical transport model using the results of the meteorological simulation.
b. Chemical transport model (CTM) part of NHM-Chem

Table S2. List of MIR for the SUPRC-99 VOC group (derived regarding Carter, 2000)

Name	name description in NHM-Chem	weighted MIR ($g\text{-}O_3$/ g-NMVOC)	weighted MIR ($mol\text{-}O_3$/ mol-NMVOC)	species	Weight %	MIR ($g\text{-}O_3$/g-NMVOC)	MWT (g-NMVOC/mol-NMVOC)
hcho	formaldehyde	9.27	5.80	formaldehyde	100.0	9.27	30.03
meoh	methanol	0.77	0.51	methanol	100.0	0.77	32.04
mek	ketones and other non-aldehyde oxygenated products (slower with OH)	1.70	3.05	Cyclobutanone	12.5	0.77	70.09
				Methyl Ethyl Ketone	12.5	1.59	72.11
				Cyclopentanone	12.5	1.51	84.12
				3-Pentanone	12.5	1.55	86.13
				2-Pentanone	12.5	3.34	86.13
				Methyl t-Butyl Ketone	12.5	0.86	100.16
				Hydroxy Acetone	12.5	3.22	74.08
				Diacetone Alcohol	12.5	0.76	116.16
prod2	ketones and other non-aldehyde oxygenated products (faster with OH than 5e-12 cm3/molec2/sec)	2.45	6.02	Cyclohexanone	9.1	1.76	98.15
				4-Methyl-2-Pentanone	9.1	4.62	100.16
				Methyl n-Butyl Ketone	9.1	3.82	100.16
				Di-Isopropyl Ketone	9.1	1.80	114.19
				2-Methyl-3-Hexanone	9.1	1.98	114.19
				2-Heptanone	9.1	3.05	114.19
				2-Octanone	9.1	1.81	128.22
				2-Nonanone	9.1	1.42	142.24
				Di-isobutyl ketone (2,6-dimethyl-4-heptanone)	9.1	3.22	142.24
				2-Decanone	9.1	1.14	156.27
				Methoxy Acetone	9.1	2.33	88.11
cco_oh	acetic acid	0.83	1.05	Acetic Acid	100.0	0.83	60.5
ccho	acetaldehyde	7.25	6.65	acetaldehyde	100.0	7.25	44.05
acet	acetone	0.45	0.54	Acetone	100.0	0.45	58.08
phen	phenol	1.89	3.71	Phenol	100.0	1.89	94.11
hcooh	formic acid	0.09	0.05	Formic Acid	100.0	0.09	30.03
rcho	lumped c3 + aldehydes	5.65	11.03	Propionaldehyde	6.7	8.43	58.08
				2-Methylpropanal	6.7	6.30	72.11
				Butanal	6.7	7.15	72.11
				Pentanal	6.7	6.10	86.13
				2,2-Dimethylpropanal	6.7	5.78	86.13
				3-Methylbutanal	6.7	5.91	86.13
				Glutaraldehyde	6.7	5.18	100.12
				Hexanal	6.7	5.17	100.16
				Heptanal	6.7	4.40	114.19
				Octanal	6.7	3.79	128.22
				C4 aldehydes	6.7	7.15	72.11
				C5 aldehydes	6.7	6.10	86.14
				C6 aldehydes	6.7	5.17	100.16
				C7 aldehydes	6.7	4.40	114.19
				C8 aldehydes	6.7	3.79	128.22
gly	glyoxal	14.81	17.91	Glyoxal	100.0	14.81	58.04
mgly	methyl glyoxal	16.99	25.51	Methyl Glyoxal	100.0	16.99	72.07
bacl	biacetyl	21.75	39.01	Biacetyl	100.0	21.75	86.09
cres	cresols	2.41	5.43	m-cresol	33.3	2.41	108.14
				p-cresol	33.3	2.41	108.14
				o-cresol	33.3	2.41	108.14
bald	aromatic aldehydes (e.g. benzaldehyde)	-0.51	-1.13	Benzaldehyde	100.0	-0.51	106.13
methacro	methacrolein	6.67	9.74	Methacrolein	100.0	6.67	70.09
mvk	methyl vinyl ketone	10.05	15.10	Methylvinyl ketone	100.0	10.05	72.11
isoprod	lumped isoprene product species	8.53	13.87	Crotonaldehyde	50.0	10.34	70.09
				Hydroxy Methacrolein	50.0	6.71	86.09
ethene	ethene	9.53	5.57	ethene	100.0	9.53	28.05
isoprene	isoprene	11.48	16.29	isoprene	100.0	11.48	68.12
trp1	terpens	4.05	11.61	a-Pinene	38.0	4.51	136.24

				b-Pinene	27.0	3.58	136.24
				3-Carene	17.0	3.47	136.24
				Sabinene	10.0	3.96	136.24
				d-Limonene	9.0	4.25	136.24
ALK1	alkanes and other non-aromatic comp., react only with OH, kOH < 5.e2 /ppm/min) :: almost ethane	0.35	0.22	ethane	100.0	0.35	30.07
ALK2	alkanes and other non-aromatic comp., react only with OH, kOH < 2.5e3	0.91	0.70	propane	59.0	0.64	44.1
				acetylene	41.0	1.31	26.04
ALK3	alkanes and other non-aromatic comp., react only with OH, kOH < 5.e3	1.48	1.81	n-butane	68.0	1.48	58.12
				isobutane	30.0	1.48	58.12
				2,2-dimethylbutane	2.0	1.45	86.18
ALK4	alkanes and other non-aromatic comp., react only with OH, kOH < 1. e4	1.95	3.18	isopentane	45.0	1.87	72.15
				n-pentane	18.0	1.77	72.15
				2-methylpentane	11.0	2.02	86.18
				3-methyl pentane	8.0	2.33	86.18
				2,4-dimethylpentane	5.0	1.90	100.21
				methylcyclopentane	5.0	2.46	84.16
				n-hexane	4.0	1.71	86.18
				2,3-dimethyl butane	3.0	1.28	86.18
				cyclopentane	2.0	2.65	70.14
ALK5	alkanes and other non-aromatic comp., react only with OH, kOH > 1. e4	1.53	3.65	2,4-Dimethyl Hexane	11.0	2.13	114.23
				n-Decane	10.0	0.97	142.29
				3-Methyl Hexane	10.0	1.66	100.21
				n-Heptane	7.0	1.48	100.21
				2,3-Dimethyl Pentane	6.0	1.75	100.21
				2-Methyl Heptane	6.0	2.02	114.23
				4-Methyl Heptane	6.0	1.67	114.23
				2,4-Dimethyl Heptane	5.0	1.75	128.26
				Methylcyclohexane	4.0	2.09	98.19
				2,6-Dimethyl Octane	4.0	1.44	142.29
				n-Nonane	4.0	1.10	128.26
				n-Octane	4.0	1.28	114.23
				Cyclohexane	4.0	2.02	84.16
				2-Methyl Hexane	3.0	1.74	100.21
				4-Methyl Octane	2.0	1.31	128.26
				2-Methyl Octane	2.0	1.15	128.26
				4-Methyl Nonane	2.0	1.18	142.29
				2-Methyl Nonane	2.0	1.02	142.29
				n-Dodecane	2.0	0.81	170.34
				Ethylcyclohexane	1.0	1.95	112.22
				n-Undecane	1.0	0.88	156.31
				3,6-Dimethyl Decane	1.0	1.03	170.34
ARO1	aromatics with kOH < 2.e4 /ppm/min	3.64	7.00	Toluene	70.0	4.24	92.14
				n-Propyl Benzene	10.0	2.40	78.11
				Ethyl Benzene	10.0	3.03	106.17
				Benzene [a]	7.0	0.91	78.11
				s-Butyl Benzene	2.0	2.15	134.22
				Isopropyl Benzene (cumene)	1.0	2.53	120.2
ARO2	aromatics with kOH > 2.e4 /ppm/min	9.06	21.21	m-Xylene	22.0	11.40	106.17
				p-Xylene	22.0	4.56	106.17
				o-Xylene	20.0	7.87	106.17
				1,3,5-Trimethyl Benzene	14.0	11.76	120.2
				1,2,3-Trimethyl Benzene	14.0	11.74	120.2
				1,2,4-Trimethyl Benzene	9.0	7.57	120.2
ORE1	alkenes with kOH < 7.e4 /ppm/min	8.19	12.42	Propene	29.0	12.19	42.08
				1-Hexene	24.0	6.09	84.16

	(other than ethene)			1-Butene	12.0	10.91	56.11
				1-Pentene	11.0	8.00	70.14
				1-Heptene	11.0	4.49	98.19
				1-Nonene	5.0	2.82	126.24
				3-Methyl-1-Butene	3.0	7.72	70.14
				1-Octene	2.0	3.42	112.22
				1-Undecene	2.0	2.09	154.3
				1-Decene	1.0	2.39	140.27
ORE2	alkenes with kOH > 7.e4 /ppm/min	9.49	14.74	trans-2-Pentene	13.0	10.86	70.14
				cis-2-Pentene	13.0	10.86	70.14
				trans-2-Butene	10.0	14.51	56.11
				Isobutene	10.0	6.59	56.11
				cis-2-Butene	8.0	13.81	56.11
				2-Methyl-1-Butene	8.0	6.78	70.14
				Styrene	7.0	2.17	104.15
				1,3-Butadiene	5.0	12.88	54.09
				2-Methyl-2-Butene	4.0	14.97	70.14
				Trans-2-Hexene	4.0	8.69	84.16
				Cis-2-Hexene	4.0	8.69	84.16
				Trans-3-Heptene	4.0	7.26	84.16
				Trans-4-Nonene	2.0	4.96	128.26
				Trans-4-Octene	2.0	6.02	112.22
				Trans-2-Heptene	2.0	7.10	98.19
				Trans-5-Undecene	2.0	3.73	154.3
				Cyclohexene	1.0	5.47	82.15
				Trans-4-Decene	1.0	4.27	140.27